ZKCM: a C++ library for multiprecision matrix computation with applications in quantum information

Akira SaiToh[a,*]

[a]*Quantum Information Science Theory Group, National Institute of Informatics, 2-1-2 Hitotsubashi, Chiyoda, Tokyo 101-8430, Japan*

Abstract

ZKCM is a C++ library developed for the purpose of multiprecision matrix computation, on the basis of the GNU MP and MPFR libraries. It provides an easy-to-use syntax and convenient functions for matrix manipulations including those often used in numerical simulations in quantum physics. Its extension library, ZKCM_QC, is developed for simulating quantum computing using the time-dependent matrix-product-state simulation method. This paper gives an introduction about the libraries with practical sample programs.

Keywords: multiprecision computing; linear algebra; time-dependent matrix product state; quantum information

PROGRAM SUMMARY

Manuscript Title: ZKCM: a C++ library for multiprecision matrix computation with applications in quantum information
Authors: Akira SaiToh
Program Title: ZKCM
Journal Reference:
Catalogue identifier:
Licensing provisions: GNU Lesser General Public License Ver. 3
Programming language: C++
Computer: General computers
Operating system: Unix-like systems, such as Linux, Free BSD, Cygwin on Windows OS, etc.
RAM: Several mega bytes - several giga bytes, dependent on the problem instance
Keywords: Multiprecision computing, Linear algebra, Time-dependent matrix product state, Quantum information
Classification: 4.8 Linear Equations and Matrices, 4.15 Quantum Computing
External routines/libraries: GNU MP (GMP) [1], MPFR [2] Ver. 3.0.0 or later
Nature of problem: Multiprecision computation is helpful to guarantee and/or evaluate the accuracy of simulation results in numerical physics. There is a potential demand for a programming library focusing on matrix computation usable for this purpose with a user-friendly syntax.
Solution method: A C++ library ZKCM has been developed for multiprecision matrix computation. It provides matrix operations useful for numerical studies of physics, e.g., the tensor product (Kronecker product), the tracing-out operation, the inner product, the LU decomposition, the Hermitian-matrix diagonalization, the singular-value decomposition, and the discrete Fourier transform. For basic floating-point operations, GMP and MPFR libraries are used. An extension library ZKCM_QC has also been developed, which employs the time-dependent matrix-product-state method to simulate quantum computing.
Restrictions: Multiprecision computation with more than a half thousand bit precision is often a thousand times slower than double-precision computation for any kind of matrix computation.
Additional comments: A user's manual is placed in the directory "doc" of the package. Each function is explained in a reference manual found in the directories "doc/html" and "doc/latex". Sample programs are placed in the directory "samples".
Running time: It takes less than thirty seconds to obtain a DFT spectrum for 2^{16} data points of a time evolution of a quantum system described by a 4×4 matrix Hamiltonian for 256-bit precision when we use recent AMD or Intel CPU with 2.5 GHz or more CPU frequency. It takes three to five minutes to diagonalize a 100×100 Hermitian matrix for 512-bit precision using the aforementioned CPU.

References

[1] The GNU Multiple Precision Arithmetic Library, http://gmplib.org/.
[2] L. Fousse *et al.*, MPFR: A multiple-precision binary floating-point library with correct rounding, ACM Trans. Math. Software 33 (2007) 13, http://www.mpfr.org/.

1. Introduction

Precision of floating-point operations is sometimes of serious concern in simulation physics when rounding errors in variables or matrix elements considerably affect numerical results for investigated physical phenomena [1]. There are several programming libraries, e.g., Refs. [2, 3, 4, 5, 6, 7], for high-precision computing, which are helpful in this regard. Among them, the library named

*Corresponding author.
E-mail address:* akirasaitoh@nii.ac.jp

ZKCM [7], which we have been developing, is a C++ library for multiprecision complex-number matrix computation. It provides several functionalities including the LU decomposition, the singular value decomposition, the tensor product, and the tracing-out operation and an easy-to-use syntax for basic operations. It is based on the GNU MP (GMP) [8] and MPFR [9] libraries, which are commonly included in recent distributions of UNIX-like systems.

There is an extension library named ZKCM_QC. This library is designed for simulating quantum computing [10, 11] by the time-dependent matrix-product-state method [12] [or, simply referred to as the matrix-product-state (MPS) method]. It uses a matrix product state [13, 14, 12] to represent a pure quantum state. The MPS method is recently one of the standard methods for simulation-physics software [15]. As for other methods effective for simulating quantum computing, see, e.g., Refs. [16, 17]. With ZKCM_QC, one may use quantum gates in U(2), U(4), and U(8) as elementary gates. Indeed, in general, quantum gates in U(2) and U(4) are enough for universal quantum computing [18], but we regard quantum gates in U(8) also as elementary gates so as to reduce computational overheads in circuit constructions.

A simulation of quantum computing with MPS is known for its computational efficiency in case the Schmidt ranks are kept small during the simulation [12, 19]. Even for the case slightly large Schmidt ranks are involved, it is not as expensive as a simple simulation. The theory of MPS simulation will be briefly explained in Sec. 4.1. Numerical errors will be phenomenologically discussed in Sec. 4.3, which will give a certain reason why we introduce multiprecision computation for an MPS simulation of quantum computing.

This contribution is intended to provide a useful introduction for programming with the libraries. Section 2 describes two examples of the use of the ZKCM library: one for showing the precision dependence of a solution of a simple linear equation; the other for simulating an NMR spectrum in a simple model. Performance evaluation of the library is made in Sec. 3. Section 4 shows an overview of the theory of the MPS method and an example of simulating a simple quantum circuit using the ZKCM_QC library. In addition, later in the section numerical errors in an MPS simulation of quantum computing are examined using a certain setup of a quantum algorithm. We discuss on the effectiveness and the performance of our libraries in Sec. 5. Section 6 summarizes our achievements.

2. ZKCM Library

The ZKCM library is designed for general-purpose matrix computation. This section concentrates on its main library. It has two major C++ classes: "zkcm_class" and "zkcm_matrix". The former class is a class of a complex number. Many operators like "+=" and functions like

trigonometric functions are defined for the class. The latter class is a class of a matrix. Standard operations and functions like matrix inversion are defined. In addition, the singular-value decomposition of a general matrix, the diagonalization of an Hermitian matrix, the discrete Fourier transform, etc., are defined for the class. Functoins for the tensor product (Kronecker product) and the tracing-out operation (e.g., one can trace out the subsystem B of system ABC) are also defined. A detailed document is placed in the "doc" directory of the package of ZKCM.

As for installation of the library, the standard process "./configure → make → sudo make install" works in most cases; otherwise the document should be consulted.

We will next look at simple examples to demonstrate the programming style using the library. (Here, the latest stable version, ver. 0.3.2, is used.)

2.1. Program examples

Example 1. There is a classical example [20] often mentioned to recall the importance of multiprecision computation. It clarifies that a sufficiently large precision is required even for a simple linear equation with only two variables.

Consider the linear equation

$$A \begin{pmatrix} x \\ y \end{pmatrix} = \begin{pmatrix} 1 \\ 0 \end{pmatrix}$$

with

$$A = \begin{pmatrix} 64919121 & -159018721 \\ 41869520.5 & -102558961 \end{pmatrix}.$$

The exact solution is $x = 205117922, y = 83739041$.

One way to numerically find the solution is to compute $(x, y)^t = A^{-1}(1, 0)^t$ using the matrix inversion. Another way is to utilize the Gaussian elimination (see, e.g., Refs. [21, 22]). We used functions "inv" and "gauss" of ZKCM for the former and the latter ways, respectively (as for pivoting, a partial pivoting is used in "gauss"). Then, we plotted the computed value of x against the precision [bits] as shown in Fig. 1. (Here, we refer to the number of bits for a significand of a floating-point number as precision.[1]) We can see that low-precision computing resulted in a wrong answer while high-precision computing resulted in a correct answer. It should be emphasized that the double precision (namely, 53 bits for the mantissa portion of a floating-point number) is not enough in this example.

---

[1] Precision is defined as an exact length of the mantissa portion of a floating-point number in MPFR while it is defined as a least length in GMP [9]. In ZKCM, a complex number keeps each part internally as an MPFR variable so that precision is an exact length. However, it should be noted that an output from a function usually carries over the best precision among those of involved variables in ZKCM.
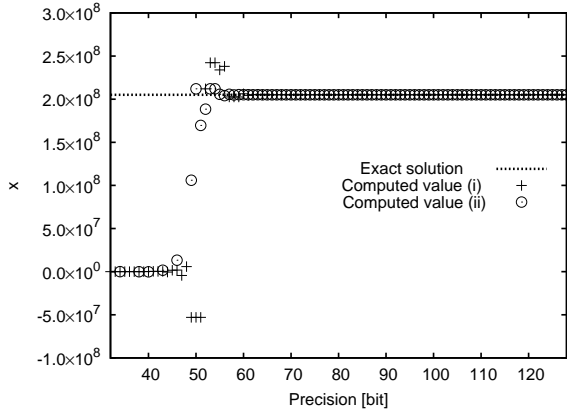
Figure 1: Plot of the computed values of x against the precision (the bit length of a mantissa) employed for floating-point numbers. Either (i) the matrix inversion (pluses) or (ii) the Gaussian elimination (circles) was used. For case (ii), there are data points with x values $< -1.0 \times 10^8$ for some values of precision < 50; they are outside the range in the figure.

The program used for this example is shown in Listing 1. It is found as "samples/classic_example.cpp" in the package. It is written to use the matrix inversion. To use the Gaussian elimination, the line "B = inv(A) * B;" should be replaced with "B = gauss(A, B);".

```
#include "zkcm.hpp"
#include <fstream>
int main()
{
  std::ofstream ofs("classic_example.dat");
  if (!ofs)
  {
    std::cerr << "Could not create the file\
 classic_example.dat"
              << std::endl;
    return -1;
  }
  ofs << "# prec x y" << std::endl;
  for (int prec = 32; prec < 257; prec++)
  {
    zkcm_set_default_prec(prec);
    zkcm_matrix A(2, 2), B(2, 1);

    A(0, 0) = "64919121";
    A(0, 1) = "-159018721";
    A(1, 0) = "41869520.5";
    A(1, 1) = "-102558961";

    B(0, 0) = 1;
    B(1, 0) = 0;

    B = inv(A) * B;
    //Replace the above line with
    //B = gauss(A, B);
    //to use the Gaussian elimination instead.

    ofs << prec << " "
        << B(0, 0) << " "
        << B(1, 0) << std::endl;
  }
  zkcm_quit();
  return 0;
```

```
}
```

Listing 1: classic_example.cpp

The program is compiled and executed in a standard way.[2] Its output file "classic_example.dat" can be visualized by Gnuplot [23] using the file "classic_example.gnuplot" found in the "samples" directory.

In the program, one can see typical features of the ZKCM library. The line "zkcm_set_default_prec(prec);" sets the default internal precision (the default bit length of a significand) of an object to "prec". Any object like "A" (this is a 2×2 matrix) constructed without specified precision possesses the default precision. It is possible to specify a particular precision (*i.e.*, in case of a matrix object, the length of the significand for each part of each element of the matrix), say, 512, by constructing the object as "zkcm_matrix A(2, 2, 512)", for instance. For a matrix object, say, "A", it is convenient to access its (i, j) element by "A(i,j)" that is a reference to the element. The element is an object in the type of "zkcm_class". To assign a value into a "zkcm_class" object (a complex number) "z", one can write "z=...;" where the right-hand side can be a number or a string describing a complex number in the style "___+___*I" (PARI/GP style [24]; here, "I" stands for $i = \sqrt{-1}$), "___+___i", "___+___j" (here, "j" stands for i), etc. (there are other acceptable styles). In the program, by "A(0, 0) = "64919121";" the value $64919121 + 0i$ is assigned to the $(0,0)$ element of matrix A. Other values are assigned to corresponding elements in a similar way. The solution of the linear equation is obtained by using the function "inv" or "gauss". The obtained result is written into the output file stream "ofs" by using the operator "<<". In the program, the elements are individually written out so as to meet the data format of a data-plotting program. After computation is performed, the program should be terminated. At this stage, it is recommended to write "zkcm_quit();" so as to release miscellaneous memories allocated for internal use of background library functions.

Example 2. As the second example, a sample program "NMR_spectrum_simulation.cpp" found in the "samples" directory of the package of ZKCM is explained. This program generates a simulated free-induction-decay (FID) spectrum of liquid-state NMR for the spin system consisting of a proton spin with precession frequency $w_1 = 400$ MHz (variable "w1" in the program) and a ^{13}C spin with precession frequency $w_2 = 125$ MHz (variable "w2") at room temperature (300 K) (variable "T"). A J coupling constant $J_{12} = 140$ kHz (variable "J12") is considered for the spins.

---

[2]To make an executable file, the library flags typically "-lzkcm -lm -lmpfr -lgmp -lgmpxx" are required. As for ZKCM_QC, additionally "-lzkcm_qc" should be specified.

The first line of the program is to include a header file of ZKCM:

```
#include "zkcm.hpp"
int main(int argc, char *argv[])
{
```

In the beginning of the "main" function, the default precision is set to 280 bits by

```
zkcm_set_default_prec(280);
```

In the subsequent lines, some matrices like Pauli matrices I and X, etc. are generated. For example, X is generated as

```
zkcm_matrix X = "[0, 1; 1, 0]";
```

using a string representing a matrix in the PARI/GP style. The Y_{90} pulse is generated as

```
zkcm_matrix Yhpi(2,2);
Yhpi(0,0) = sqrt(zkcm_class(0.5));
Yhpi(0,1) = sqrt(zkcm_class(0.5));
Yhpi(1,0) = -sqrt(zkcm_class(0.5));
Yhpi(1,1) = sqrt(zkcm_class(0.5));
```

Other matrices are generated by similar lines. After this, values of constants and parameters are set. For example, the Boltzmann constant k_B [J/K] is generated as

```
zkcm_class kB("1.3806504e-23");
```

The Hamiltonian H of the spin system is generated in the type of "zkcm_matrix" and is specified as

```
H = w1 * tensorprod(Z/2,I) + w2 * tensorprod(I,Z/2)
    + J12 * tensorprod(Z/2,Z/2);
```

This is used to generate a thermal state ρ:

```
zkcm_matrix rho(4,4);
rho = exp_H((-hplanck/kB/T) * H);
rho /= trace(rho);
```

Here, "exp_H" is a function to calculate the exponential of an Hermitian matrix and "hplanck" is the Planck constant $(6.62606896 \times 10^{-34}$ Js). The sampling time interval dt to record the value of $< X >$ for the proton spin is set to $0.43/w_1$ (any number smaller than $1/2$ might be fine instead of 0.43) by

```
zkcm_class dt(zkcm_class("0.43")/w1);
```

The number of data to record is then decided as

```
int N = UNP2(8.0/dt/J12);
```

Here, function "UNP2" returns the integer upper nearest power of 2 for a given number. Now arrays to store data are prepared as row vectors.

```
zkcm_matrix array(1, N), array2(1, N);
```

The following lines prepare the X and Y_{90}-pulse operators acting only on the proton spin.

```
zkcm_matrix X1(4, 4), Yhpi1(4, 4);
X1 = tensorprod(X, I);
Yhpi1 = tensorprod(Yhpi, I);
```

To get an FID data, we firstly tilt the proton spin by the ideal Y_{90} pulse.

```
rho = Yhpi1 * rho * adjoint(Yhpi1);
```

Now the data of time evolution of $< X >$ of the proton spin under the Hamiltonian H is recorded for the time duration N × dt using

```
array = rec_evol(rho, H, X1, dt, N);
```

We now use a zero-padding for this "array" so as to enhance the resolution. This will extend the array by N zeros.

```
array2 = zero_padding(array, 2*N);
```

To obtain a spectrum, the discrete Fourier transform is applied.

```
array2 = abs(DFT(array2));
```

This "array2" is output to the file "example_zp.fid" as an FID spectrum data with $df = 1/(2 \times N \times dt)$ as the frequency interval, in the Gnuplot style by

```
GP_1D_print(array2, 1.0/dt/zkcm_class(2*N),
            1, "example_zp.fid");
```

At last, the function "main" ends with "zkcm_quit();" and "return 0;". The program is compiled and executed in a standard way.

The result stored in "example_zp.fid" is visualized by Gnuplot using the file "example_zp.gnuplot" placed in the directory "samples", as shown in Fig. 2.
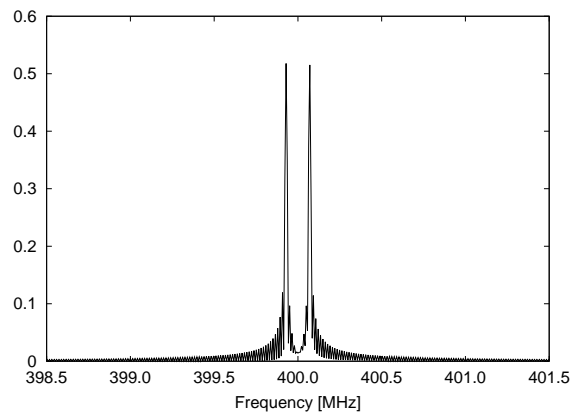

Figure 2: Plot of the simulation data stored in "example_zp.fid". See the text for the details of this simulation.

It should be noted that we have not employed a high-temperature approximation. Under a high-temperature approximation, the first order deviation $-\beta H$

4

of $\exp(-\beta H)$ (here, $\beta = h/(k_{\mathrm{B}}T)$) is considered as a deviation density matrix and calculations are performed using the normalized deviation density matrix $-H/\text{const}$. This approximation is commonly used [28] but it cannot be used for simulations for low temperature. An advantage of using ZKCM for simulating NMR spectra is that the temperature can be chosen. This is possible because of high accuracy in computing the exponential of a Hamiltonian.

As we have seen in this example, ZKCM has useful functions to handle matrices, especially those often used in simulations in quantum physics. For the list of available functions, see the reference manual found in the package.

3. Performance evaluation

We evaluate the performance of ZKCM (version 0.3.2) in comparison with PARI [24] (version 2.5.3 with the GMP kernel), a conventional highly-evaluated C library for mathematical computing.

3.1. Speed of computing the Γ function

Here, we evaluate the performance of the function "gamma" of ZKCM, which calculates $\Gamma(z)$ for a complex number z. It is implemented on the basis of the expansion using the Stirling formula for $\mathrm{Re}\, z \geq 0$:

$$\Gamma(z) \simeq e^{-z} z^{z-1} \sqrt{2\pi z} \exp\left[\sum_{n=1}^{L} \frac{(-1)^{n-1}|B_{2n}|z^{1-2n}}{2n(2n-1)} + R_L\right],$$

where B_m is the first or the second Bernoulli number (as the absolute value is used, either is fine); L is a sufficiently large (but not very large) integer to guarantee the accuracy; R_L is the remainder of the sum (corresponding to the sum of the terms for $n = L+1, \ldots, \infty$). It is known that the expansion is not convergent since $|B_{2n}|$ grows rapidly for large n. It was, however, proved by Spira [25] that $|R_L| \leq \frac{|B_{2L}|}{2L-1}|z|^{1-2L}$ holds when $\mathrm{Re}\, z \geq 0$. Thus the expansion is usable for computation with enough accuracy as long as z is appropriately scaled to a large value in advance. We internally scale z to satisfy $\mathrm{Re}\, z \geq 0$ and $|z| \geq 10^3 \sim 2^{10}$. In accordance with this scaling, L is appropriately chosen so that R_L becomes small enough for required precision. For the scaling, the well-known formulae $\Gamma(z) = \Gamma(z+k)/[z(z+1)\cdots(z+k-1)]$ (here, k is an integer) and $\Gamma(z) = -\pi/[z\Gamma(-z)\sin(-\pi z)]$ (here, z is not a pole) are utilized. To compute Bernoulli numbers, we utilize the relation

$$B_m = 1 - \sum_{k=0}^{n-1} \binom{n}{k} \frac{B_k}{n-k+1}$$

and the fact that B_{2j+1} vanishes for integer $j \geq 1$. We keep the computed values of binomial coefficients and Bernoulli numbers inside a certain subblock of a function for computing $\Gamma(z)$. Therefore, the cost to compute B_m assuming that we have already computed $B_0, \ldots, B_{m-2}$ for even

number m is small: $O(m)$ rational-number operations are enough[3] (we make use of the C++ class "mpq_class" of GMP for internally handling rational numbers).

Now, the speed of computing $\Gamma(z)$ using "gamma" is evaluated for $z = a + bi$ with random $a, b \in [-10, 10]$. It is compared with the function with the same name, "gamma", of the PARI library. The PARI library uses a similar algorithm to compute $\Gamma(z)$. The main difference is that PARI can utilize cached values of Bernoulli numbers that are once calculated in any function during a process is running. It can also use precomputed values of typical constants.

As shown in Table 1, the average computation time of $\Gamma(z)$ in the ZKCM library is on the same order of magnitude as that in the PARI library in the absence of cached values of Bernoulli numbers. However, in the presence of cached values of Bernoulli numbers, the computation speed of $\Gamma(z)$ in PARI is quite much faster.

3.2. Speed of matrix multiplication

Here, we evaluate the speed of matrix multiplication. We first generate a 100×100 random Hermitian matrix A satisfying $\sqrt{\mathrm{Tr}AA^\dagger} = 1$. We then continue to compute the operations (i) $A \leftarrow A^2$ and (ii) $A \leftarrow A/\sqrt{\mathrm{Tr}AA^\dagger}$ sequentially, i.e., (i) (ii) (i) (ii) ... from left to right. Operations are performed under a specified precision "prec". We compare time consumption to perform ten sets of "(i) (ii)". Time spent for the matrix preparation is not included. As shown in Table 2, computation time is on the same order of magnitude for ZKCM and PARI and discrepancy in time consumption is not large. This result is plausible since both the libraries employ a straight-forward way to implement matrix multiplication and rely on the GMP library for the speed of primitive operations. (ZKCM uses MPFR for basic operations that is based on GMP; hence ZKCM indirectly uses primitive operations of GMP.)

3.3. Speed of Hermitian-matrix diagonalization

We next evaluate the speed of diagonalization of an Hermitian matrix for finding all the eigenvectors. The

---

[3] For other use than computing $\Gamma(z)$, we cannot use this assumption in general. In this case, Akiyama-Tanigawa algorithm [26] is employed to calculate the Bernoulli number. This takes $O(m^2)$ rational-number operations.

[4] This was because the improvement in running time due to setting compiler optimization flags was negligible. (Of course, there were other compiler flags for library specifications etc. which are not of our concern in this context.) For instance, a program to find eigenvectors of a normalized random 50×50 Hermitian matrix using the function "diag_H" of ZKCM ("eigen" of PARI) with 768-bit precision consumed 34.558 (14.550) seconds on average when compiled without optimization flags, and consumed 34.314 (14.551) seconds on average when compiled with the optimization flags "-O3 -fno-strict-aliasing -fomit-frame-pointer". (Here, we used the Frobenius norm for normalization.) The average was taken over 100 trials. The standard deviations were 0.0648 (0.143) and 0.0645 (0.122), respectively. The compiler was GCC ver. 4.6.3 installed by default on the operating system Fedora 15 64-bit. A computer with the Intel Core i5 M460 2.53 GHz CPU (maximum clock frequency 2.80GHz) and 4GB RAM was used.

Table 1: Comparison of the average real time consumption for computing $\Gamma(z)$ for $z = a + bi$ with random $a, b \in [-10, 10]$. The average was taken over 1,000 trials. No I/O operation was involved. Time for generating z was negligible (this was no more than 2.0×10^{-5} seconds). The standard deviation (we employ the sample standard deviation) for each entry is shown in small fonts under the entry. "prec" stands for the precision (the bit length of each mantissa) employed in a program. In a program using PARI, function "nbits2prec" was used to convert the precision into the number of code words that is defined as the precision for variables in PARI. ZKCM version 0.3.2 and PARI version 2.5.3 were used. They were compiled with GCC/G++ with their default optimization flags, while test programs for this performance evaluation were compiled without optimization flags.[4] In this table, the middle and the right columns show the results for PARI with and without precomputed values of Bernoulli numbers, respectively. Environments: For upper entries (♦): Fedora 15 64-bit operating system on Intel Core i5 M460 CPU (2.53 GHz, Max. 2.80GHz) with 4GB RAM. For lower entries (♣): Fedora 16 64-bit operating system on AMD FX-8120 CPU (3.10GHz, Max. 4.00GHz) with 16GB RAM.

prec	ZKCM [sec]	PARI without cache [sec]	PARI with cache [sec]
256	♦3.73×10^{-3}	1.38×10^{-3}	1.63×10^{-4}
	(8.72×10^{-5})	(7.91×10^{-5})	(6.10×10^{-5})
	♣2.95×10^{-3}	1.42×10^{-3}	1.48×10^{-4}
	(9.58×10^{-5})	(2.73×10^{-4})	(9.56×10^{-5})
512	9.04×10^{-3}	4.70×10^{-3}	3.43×10^{-4}
	(2.95×10^{-4})	(6.79×10^{-4})	(1.49×10^{-4})
	7.15×10^{-3}	3.12×10^{-3}	3.43×10^{-4}
	(1.64×10^{-4})	(6.78×10^{-4})	(1.75×10^{-4})
768	1.86×10^{-2}	9.58×10^{-3}	6.61×10^{-4}
	(2.62×10^{-4})	(1.82×10^{-3})	(3.67×10^{-4})
	1.45×10^{-2}	8.38×10^{-3}	6.02×10^{-4}
	(2.80×10^{-4})	(1.85×10^{-3})	(2.07×10^{-4})
1024	3.48×10^{-2}	1.48×10^{-2}	1.25×10^{-3}
	(8.77×10^{-4})	(8.32×10^{-4})	(3.39×10^{-4})
	2.59×10^{-2}	1.34×10^{-2}	1.03×10^{-3}
	(3.67×10^{-4})	(6.35×10^{-4})	(3.64×10^{-4})
1280	5.37×10^{-2}	2.44×10^{-2}	1.95×10^{-3}
	(1.41×10^{-3})	(9.68×10^{-4})	(6.87×10^{-4})
	3.92×10^{-2}	2.09×10^{-2}	1.70×10^{-3}
	(9.90×10^{-4})	(1.56×10^{-3})	(7.23×10^{-4})

Table 2: Comparison of the average real time consumption to perform ten sets of operations (i) and (ii) (see the text). The average was taken over ten different A's (again, see the text). The standard deviation is shown in parentheses in small fonts. "prec" stands for the precision (the bit length of a significand). Environments: Fedora 15 OS on Intel Core i5 M460 CPU with 4GB RAM for upper entries (♦) and Fedora 16 OS on AMD FX-8120 CPU with 16GB RAM for lower entries (♣).

prec	ZKCM [sec]	PARI [sec]
256	♦26.1 (0.115)	15.0 (0.204)
	♣21.4 (0.248)	13.0 (0.567)
512	35.5 (0.206)	21.9 (0.0208)
	27.3 (0.202)	18.7 (0.188)
768	46.4 (0.161)	30.8 (0.0702)
	36.9 (0.266)	28.1 (0.247)
1024	65.8 (0.115)	50.5 (0.199)
	53.2 (0.178)	41.3 (0.434)
1280	86.5 (0.0265)	67.8 (0.118)
	69.3 (0.181)	54.9 (0.715)

functions used for this task are "diag_H" of ZKCM and "eigen" and "jacobi" of PARI.

Let us briefly explain our design of "diag_H". In the function, the routine to diagonalize an Hermitian matrix A employs a standard QR method (see, *e.g.*, Refs. [31, 32]) to find eigenvalues, for which Householder reflections and Wilkinson shifts are utilized. The eigenvalues λ_i are sorted from larger to smaller. Then each corresponding eigenvector $|v_i\rangle$ is calculated by the inverse iteration. During this process, we set

$$A \leftarrow A + \text{const.} \times |v_{i-1}\rangle\langle v_{i-1}|$$

before calculating $|v_i\rangle$. This resolves degeneracy (in case we have), so that calculated eigenvector $|v_i\rangle$ becomes orthogonal to $|v_0\rangle, \ldots, |v_{i-1}\rangle$ with high accuracy. We still test orthogonality and, in case required, perform an orthogonalization of $|v_i\rangle$'s. Enhancement in accuracy of λ_i is achieved during the inverse iteration steps. The steps are retried, often with an initial vector set to the vector found in the previous round of steps, and sometimes with a randomly chosen initial vector, until sufficient convergence of $|v_i\rangle$ and λ_i for required precision is reached.

As for the functions of PARI, "eigen" firstly computes the roots of the characteristic polynomial and secondly uses the Gaussian elimination to find eigenvectors; in contrast, "jacobi" simply uses the Jacobi method. There are known facts on PARI library functions [29]: function "eigen" uses a naive algorithm so that it fails to compute eigenvectors for matrices with degenerate eigenvalues; function "jacobi" handles real symmetric matrices only, so that an Hermitian matrix A should be reformed into a symmetric matrix $\begin{pmatrix} \text{Re}(A) & -\text{Im}(A) \\ \text{Im}(A) & \text{Re}(A) \end{pmatrix}$ (see Ch. 11.5 of Ref. [30] for details about this reformation) as a workaround to find eigenvalues and eigenvectors using

the function.

We compare the average time consumption to find all the eigenvectors of a random 100×100 Hermitian matrix A with a unit Frobenius norm for several different internal precisions. To generate A, matrix elements $a_{ij} = a_{ji}^*$ are simply randomly generated and then the normalization of the matrix is performed. The eigenvectors found by a diagonalization are the column vectors of unitary matrix U such that $U^{-1}AU = \text{diag}$.

The probability for a random matrix to be degenerate is very small. Tested matrices were in fact nondegenerate and "eigen" worked fine except for the precision 256 [bits] for which it stopped due to a low-accuracy error. As for "jacobi", we used the workaround as mentioned above so that the matrix actually input into the function was a 200×200 real symmetric matrix. In this case, we had to double the precision of the matrix in order to keep the off-diagonal elements of $\widetilde{D} = U^{-1}AU$ sufficiently small (i.e., $|\widetilde{D}_{ij,i \neq j}| \lesssim 2^{-(\text{prec}-10)}$) for the specified precision prec. This was not a theoretical consequence but an empirical workaround for the use of "jacobi". In fact, with precision 512 (1024) [bits], "jacobi" constantly achieved $|\widetilde{D}_{ij,i \neq j}| \sim 1.0 \times 10^{-78} \sim 1.0 \times 2^{-256}$ ($|\widetilde{D}_{ij,i \neq j}| \sim 1.0 \times 10^{-155} \sim 1.0 \times 2^{-512}$). Thus, it was reasonable that doubled precision was handed over to "jacobi" when it was called.

As shown in Table 3, time consumption for "diag_H" of ZKCM is on the same order of magnitude as those for the functions "eigen" and "jacobi" of PARI, as far as we tested for the precision between 256 and 1280 [bits].

In addition, we also compare the average time consumption to find all the eigenvectors of a random $N \times N$ Hermitian matrix with a unit Frobenius norm for several different values of N with fixed precision 768 [bits]. We doubled the precision for "jacobi" due to the above-mentioned reason. As shown in Table 4, time consumption of "diag_H" is on the same order of magnitude as those for "eigen" and "jacobi" as far as we tested for $25 \leq N \leq 125$.

The evaluated functions are all designed to find eigenvectors in addition to eigenvalues. One may think of the case only eigenvalues are needed, for which shorter computation time is expected. The PARI library does not have a function for this purpose. The ZKCM library has the function "eigenvalues_H" which is created by simply omitting the inverse iterations from "diag_H". The problem is that the precision of computed eigenvalues cannot be guaranteed without corresponding eigenvectors. The achievable precision in the absence of inverse iterations is evaluated as below together with the time consumption.

Numerical error in the absence of inverse iterations. The performance of "eigenvalues_H" is evaluated in Tables 5 and 6 in comparison with "diag_H". The real time consumption to find all the eigenvalues of a normalized randomly-generated $N \times N$ Hermitian matrix and the numerical error in the computed eigenvalues are used for this comparison. Here, the matrix was generated by a random

Table 3: Comparison of the average real time consumption to find all the eigenvectors of a normalized random 100×100 Hermitian matrix. The average was taken over ten different matrices. The standard deviation is shown in parentheses in small fonts. "prec" stands for the precision. Environments: Fedora 15 OS on Intel Core i5 M460 CPU with 4GB RAM for upper entries (♦) and Fedora 16 OS on AMD FX-8120 CPU with 16GB RAM for lower entries (♣). Note: For precision 256 [bits], function "eigen" of PARI stopped with an error and output no result. * Precision was doubled for "jacobi" (see the text).

prec*	ZKCM, diag_H [sec]	PARI, eigen [sec]	PARI, jacobi [sec]
256	♦175 (0.105) ♣137 (0.769)	N/A (N/A) N/A (N/A)	103 (0.324) 91.2 (0.372)
512	259 (0.160) 203 (1.41)	171 (1.27) 145 (0.426)	265 (0.974) 202 (0.502)
768	413 (0.378) 330 (4.14)	237 (1.24) 206 (0.764)	477 (2.10) 367 (5.43)
1024	632 (0.358) 501 (4.14)	378 (1.58) 309 (1.14)	726 (2.24) 506 (3.65)
1280	903 (0.315) 704 (3.53)	503 (1.21) 404 (1.13)	1020 (5.47) 734 (7.98)

Table 4: Comparison of the average real time consumption to find all the eigenvectors of a normalized random $N \times N$ Hermitian matrix under the fixed precision 768 [bits] [precision was doubled for "jacobi" (see the text)]. The average was taken over ten different matrices. The standard deviation is shown in parentheses in small fonts. Environments: Fedora 15 OS on Intel Core i5 M460 CPU with 4GB RAM for upper entries (♦) and Fedora 16 OS on AMD FX-8120 CPU with 16GB RAM for lower entries (♣).

N	ZKCM, diag_H [sec]	PARI, eigen [sec]	PARI, jacobi [sec]
25	♦3.41 (0.0152) ♣2.68 (0.0130)	0.941 (0.00406) 0.841 (0.0399)	5.99 (0.0699) 4.79 (0.0219)
50	34.5 (0.0624) 27.1 (0.174)	14.5 (0.0248) 12.8 (0.0483)	50.9 (0.364) 40.9 (0.114)
75	146 (0.238) 114 (0.604)	74.3 (0.636) 64.9 (0.345)	182 (0.977) 144 (0.390)
100	413 (0.378) 330 (4.14)	237 (1.24) 206 (0.764)	477 (2.10) 367 (5.43)
125	961 (1.10) 752 (4.73)	596 (1.72) 508 (2.14)	1070 (7.40) 754 (4.62)

Table 5: Comparison of the average real time consumption for "eigenvalues_H" and "diag_H" to find all the eigenvalues of a normalized random 100×100 Hermitian matrix. The average numerical error in the computed spectrum is also shown in the columns "Error". The average was taken over ten different matrices. In each cell, the standard deviation is shown in parentheses in small fonts. "prec" stands for the precision. Environments: Fedora 15 OS on Intel Core i5 M460 CPU with 4GB RAM for upper entries (♦) and Fedora 16 OS on AMD FX-8120 CPU with 16GB RAM for lower entries (♣).

	eigenvalues_H		diag_H	
prec	Time [sec]	Error	Time [sec]	Error
256	♦9.24	1.70×10^{-32}	173	7.24×10^{-76}
	(0.250)	(2.98×10^{-32})	(1.05)	(8.69×10^{-76})
	♣7.26	1.19×10^{-32}	136	3.83×10^{-76}
	(0.149)	(2.00×10^{-32})	(1.13)	(2.01×10^{-76})
512	13.2	1.32×10^{-49}	259	3.86×10^{-153}
	(0.194)	(2.99×10^{-49})	(1.60)	(1.26×10^{-153})
	10.4	3.63×10^{-49}	202	3.96×10^{-153}
	(0.142)	(6.70×10^{-49})	(1.88)	(2.00×10^{-153})
768	19.1	9.35×10^{-57}	413	3.01×10^{-230}
	(0.368)	(8.62×10^{-57})	(2.61)	(1.12×10^{-230})
	15.2	3.71×10^{-56}	327	4.88×10^{-230}
	(0.272)	(8.16×10^{-56})	(2.82)	(5.43×10^{-230})
1024	27.6	2.08×10^{-56}	637	4.03×10^{-307}
	(0.454)	(3.71×10^{-56})	(3.27)	(3.58×10^{-307})
	22.1	4.00×10^{-56}	498	3.55×10^{-307}
	(0.346)	(7.49×10^{-56})	(2.99)	(3.01×10^{-307})
1280	35.9	6.00×10^{-56}	904	6.65×10^{-384}
	(0.871)	(9.69×10^{-56})	(4.00)	(1.18×10^{-383})
	28.4	9.84×10^{-54}	706	2.11×10^{-384}
	(0.539)	(3.10×10^{-53})	(4.64)	(6.12×10^{-385})

Table 6: Comparison of "eigenvalues_H" and "diag_H" in real time consumption to find all the eigenvalues of a normalized random $N \times N$ Hermitian matrix, for several different matrix sizes N for the fixed precision 768 [bits]. The average over ten trials is shown. The columns "Error" show the average numerical error in the computed spectrum. The standard deviation is shown in parentheses for each value. Environments: Fedora 15 OS on Intel Core i5 M460 CPU with 4GB RAM for upper entries (♦) and Fedora 16 OS on AMD FX-8120 CPU with 16GB RAM for lower entries (♣).

	eigenvalues_H		diag_H	
N	Time [sec]	Error	Time [sec]	Error
25	♦0.438	4.46×10^{-57}	3.34	9.10×10^{-231}
	(0.0179)	(8.47×10^{-57})	(0.0253)	(3.84×10^{-231})
	♣0.343	3.42×10^{-57}	2.69	6.35×10^{-231}
	(0.0153)	(8.76×10^{-57})	(0.0302)	(1.72×10^{-231})
50	2.75	1.67×10^{-56}	34.0	2.28×10^{-230}
	(0.0704)	(3.14×10^{-56})	(0.220)	(2.51×10^{-230})
	2.19	9.67×10^{-57}	27.2	2.08×10^{-230}
	(0.0824)	(1.49×10^{-56})	(0.190)	(1.02×10^{-230})
75	8.44	7.30×10^{-56}	144	3.16×10^{-230}
	(0.149)	(1.58×10^{-55})	(0.762)	(3.58×10^{-230})
	6.73	2.64×10^{-56}	114	2.40×10^{-230}
	(0.163)	(3.56×10^{-56})	(0.692)	(1.03×10^{-230})
100	19.1	9.35×10^{-57}	413	3.01×10^{-230}
	(0.368)	(8.62×10^{-57})	(2.61)	(1.12×10^{-230})
	15.2	3.71×10^{-56}	327	4.88×10^{-230}
	(0.272)	(8.16×10^{-56})	(2.82)	(5.43×10^{-230})
125	36.4	1.22×10^{-55}	950	3.76×10^{-230}
	(0.794)	(2.28×10^{-55})	(5.58)	(1.75×10^{-230})
	28.4	1.52×10^{-56}	753	3.15×10^{-230}
	(0.478)	(2.08×10^{-56})	(5.25)	(8.01×10^{-231})

unitary transformation of a diagonal matrix D with random real elements, where D was normalized by its Frobenius norm in advance. The numerical error in the computed spectrum $\{e'_i\}$ for "eigenvalues_H" is quantified by $\mathrm{E}(\{e'_i\}) = \sum_i |e_i - e'_i|$ where e_i are the true eigenvalues. Here, $\{e'_i\}$ and $\{e_i\}$ are sorted in the same order (we employed the descending order). Similarly, the numerical error in the computed spectrum $\{e''_i\}$ for "diag_H" is quantified by $\mathrm{E}(\{e''_i\}) = \sum_i |e_i - e''_i|$. For each cell of the tables, we performed the same simulation ten times with different random matrices and took the average for the time consumption or the numerical error. Note that this performance evaluation was separately performed with the evaluations shown in the previous tables. The matrix size N was fixed to 100 and several values of precision were tried for Table 5; the precision was fixed to 768 [bits] and several values of N were tried for Table 6.

It has turned out that "eigenvalues_H" is faster than "diag_H" by one or two orders of magnitude to compute eigenvalues. The only difference in the internal structures of these functions is the inverse iterations to find eigenvectors and at the same time enhance the accuracy

of eigenvalues. Thus the result shows most of time consumption in "diag_H" is spent for inverse iterations. A drawback to use "eigenvalues_H" is the nonnegligible error in the computed eigenvalues. For instance, we have $< \mathrm{E}(\{e'_i\}) > \sim 10^{-49}$ when the precision is 512 [bits], *i.e.*, when the machine epsilon is $\sim 10^{-154}$. Indeed, the error is much smaller than the machine epsilon for double precision ($\sim 10^{-16}$), but is not in the acceptable range for multiprecision computation.

So far, the ZKCM library has been introduced and evaluated on its performance. An extension library for the study of quantum computation will be introduced in the next section.

4. ZKCM_QC library

The ZKCM_QC library is an extension of the ZKCM library. It has several classes to handle tensor data useful for the (time-dependent) MPS simulation of a quantum circuit. Among the classes, the "mps" class and the "tensor2" class will be used by user-side programs. The former class conceals the complicated MPS simulation process and enables writing programs in a simple manner. The latter class is used to represent two-dimensional tensors which are often simply regarded as matrices. A quantum state during an MPS simulation can be obtained as a (reduced) density matrix in the type of "tensor2". For convenience, there are functions to convert a matrix in the type of "tensor2" to the type of "zkcm_matrix" and *vice versa*. More details of the classes are explained in the document placed in the "doc" directory of the ZKCM_QC package.

It might be curious to condensed-matter physicists why multiprecision computation is needed in an MPS simulation. Indeed, truncations of Schmidt coefficients (and corresponding Schmidt vectors) have been studied as a possible source of errors [33] while precision of basic floating-point operations has not been of main concern in physics simulations using the MPS data structure. Precision shortage cannot be a main source of errors in light of truncation errors. However, it has been uncommon[5] to use a truncation of nonzero Schmidt coefficients in time-dependent MPS simulations of quantum computing [12, 19, 27]. Under this condition, precision shortage becomes the only crucial source of errors and it is hence of our main concern how much precision is required for an accurate simulation of quantum computing. We will discuss more on this issue in Sec. 4.3. In particular, we will show an example of simulating a quantum algorithm for which a truncation of at most a single nonzero Schmidt coefficient for each step results in a significant error; in addition, a precision slightly beyond the double precision is necessary for this example.

---

[5]Here, we are considering the standard quantum circuit model for quantum computing. It is not the case in a Hamiltonian-based adiabatic-evolution model [34].

As for installation of the ZKCM_QC library, the standard process "./configure $\rightarrow$ make $\rightarrow$ sudo make install" should work; if not, the document should be consulted.

We briefly overview the theory of the MPS simulation before introducing a program example.

4.1. Brief overview of the theory of time-dependent MPS simulation

Consider an n-qubit pure quantum state

$$|\Psi\rangle = \sum_{i_0 \cdots i_{n-1}=0\cdots 0}^{1\cdots 1} c_{i_0\cdots i_{n-1}} |i_0\cdots i_{n-1}\rangle$$

with $\sum_{i_0\cdots i_{n-1}} |c_{i_0\cdots i_{n-1}}|^2 = 1$. If we keep this state as data as it is, updating the data for each time of unitary time evolution spends $O(2^{2n})$ floating-point operations. To avoid such an exhaustive calculation, in the matrix-product-state method, the data is stored as a kind of compressed data. The state is represented in the form

$$|\Psi\rangle = \sum_{i_0=0}^{1} \cdots \sum_{i_{n-1}=0}^{1} \left[\sum_{v_0=0}^{m_0-1} \sum_{v_1=0}^{m_1-1} \cdots \sum_{v_{n-2}=0}^{m_{n-2}-1} \right.$$
$$Q_0(i_0, v_0)V_0(v_0)Q_1(i_1, v_0, v_1)V_1(v_1)\cdots$$
$$\cdots Q_s(i_s, v_{s-1}, v_s)V_s(v_s)\cdots$$
$$\left. \cdots V_{n-2}(v_{n-2})Q_{n-1}(i_{n-1}, v_{n-2}) \right] |i_0\cdots i_{n-1}\rangle, \quad (1)$$

where we use tensors $\{Q_s\}_{s=0}^{n-1}$ with parameters i_s, v_{s-1}, v_s (parameters v_{-1} and v_{n-1} exceptionally do not exist) and $\{V_s\}_{s=0}^{n-2}$ with parameter v_s; m_s is a suitable number of values assigned to v_s with which the state is represented precisely or well approximated. This form is one of the forms of matrix product states (MPSs). The data are kept in the tensors. We can see that neighboring tensors are correlated to each other; the data compression is owing to this structure.

Let us explain a little more details: $Q_s(i_s, v_{s-1}, v_s)$ is a tensor with $2 \times m_{s-1} \times m_s$ elements; $V_s(v_s)$ is a tensor in which the Schmidt coefficients for the splitting between the sth site and the $(s+1)$th site (*i.e.*, the positive square roots of nonzero eigenvalues of the reduced density operator of qubits $0, \ldots, s$) are stored. This implies that, by using V_s and eigenvectors $|\Phi_{v_s}^{0\ldots s}\rangle$ ($|\Phi_{v_s}^{s+1\ldots n-1}\rangle$) of the reduced density operator $\rho^{0\ldots s}$ ($\rho^{s+1\ldots n-1}$) of qubits $0, \ldots, s$ ($s+1, \ldots, n-1$), the state can also be written in the form of Schmidt decomposition

$$|\Psi\rangle = \sum_{v_s=0}^{m_s-1} V_s(v_s)|\Phi_{v_s}^{0\ldots s}\rangle|\Phi_{v_s}^{s+1\ldots n-1}\rangle. \quad (2)$$

In an MPS simulation, very small coefficients and corresponding eigenvectors can be truncated out unlike a usual Schmidt decomposition. It may happen that all the nonzero coefficients are nonnegligible. This is actually the

case in practice when we simulate quantum computing as we will discuss in Sec. 4.3. We can still enjoy a considerable data-size reduction since vanishing coefficients are truncated out.

Besides the truncation, a significant advantage to use the MPS form is that we have only to handle a small number of tensors when we simulate a time evolution under each quantum gate. For example, when we apply a unitary operation $\in$ U(4) acting on, say, qubits s and $s+1$, we have only to update the tensors $Q_s(i_s, v_{s-1}, v_s)$, $V_s(v_s)$, and $Q_{s+1}(i_{s+1}, v_s, v_{s+1})$. For the details of how tensors are updated, see Refs. [12, 27]. The simulation of a single quantum gate $\in$ U(4) spends $O(m_{\max}^3)$ floating-point operations where $m_{\max}$ is the largest value of m_s among the sites s. (Usually, unitary operations $\in$ U(2) and those $\in$ U(4) are regarded as elementary quantum gates.) A quantum circuit constructed by using at most g single-qubit and/or two-qubit quantum gates can be simulated within the cost of $O(gnm_{\max,\max}^3)$ floating-point operations, where n is the number of wires and $m_{\max,\max}$ is the largest value of $m_{\max}$ over all time steps.

The computational complexity may be slightly different for each software using MPS. In the ZKCM_QC library, we have functions to apply quantum gates $\in$ U(8) to three chosen qubits. Internally, three-qubit gates are handled as elementary gates. This makes the complexity a little larger. A simulation using the library spends $O(gnm_{\max,\max}^4)$ floating-point operations, where g is the number of single-qubit, two-qubit, and/or three-qubit gates used for constructing a quantum circuit. As the process to update the tensors to simulate a three-qubit gate has not been written in detail in the literature as far as the author knows, it is explained in Appendix A.

The MPS simulation process, which is in fact often complicated, can be concealed by the use of ZKCM_QC. One may write a program for quantum circuit simulation in an intuitive manner. Here is a very simple example. In the followings, we use version 0.1.0 of ZKCM_QC for our programs.

4.2. Program example

As a simple example, we simulate the time evolution

$$|000\rangle \overset{H}{\mapsto} \frac{1}{\sqrt{2}}(|000\rangle + |100\rangle)$$
$$\overset{\text{CNOT}}{\mapsto} \frac{1}{\sqrt{2}}(|000\rangle + |101\rangle)$$

where Hadamard operation $H = \frac{1}{\sqrt{2}}\begin{pmatrix} 1 & 1 \\ 1 & -1 \end{pmatrix}$ acts on qubit 0 and CNOT $= |00\rangle\langle00|+|01\rangle\langle01|+|10\rangle\langle11|+|11\rangle\langle10|$ acts on qubits 0 and 2. Then we see the reduced density matrix of qubits 0 and 2.

The program example is shown in Listing 2. (A slightly extended sample code is placed in the "samples" directory of the ZKCM_QC package.) It utilizes several matrices declared in the namespace "tensor2tools" (see the document placed in the "doc" directory for the details of this namespace).

```
#include "zkcm_qc.hpp"

int main (int argc, char *argv[])
{
  //Use the 256-bit precision.
  zkcm_set_default_prec(256);
  //Num. of digits for each output is set to 8.
  zkcm_set_output_nd(8);

  //First, we make an MPS representing |000>.
  mps M(3);
  std::cout << "The initial state is "
          << std::endl;
  //Print the reduced density operator of the
  //block of qubits from 0 to 2, namely, 0,1,2,
  //using the binary number representation for
  //basis vectors.
  std::cout << M.RDO_block(0, 2).str_dirac_b()
          << std::endl;

  std::cout << "Now we apply H to the 0th qubit."
          << std::endl;
  M.applyU(tensor2tools::Hadamard, 0);

  std::cout<< "Now we apply CNOT to the \
qubits 0 and 2."
          << std::endl;
  M.applyU(tensor2tools::CNOT, 0, 2);

  //The array is used to specify qubits to compute
  //a reduced density matrix. It should be
  //terminated by the constant mps::TA.
  int array[] = {0, 2, mps::TA};
  std::cout << "At this point, the reduced \
density matrix of the qubits 0 and 2 is "
          << std::endl
          << M.RDO(array).str_dirac_b()
          << std::endl;
  zkcm_quit();
  return 0;
}
```

<div align="center">Listing 2: qc_simple_example.cpp</div>

The program is compiled and executed typically in the following way.

```
[user@localhost foo]$ c++ -o qc_simple_example \
qc_simple_example.cpp -lzkcm_qc -lzkcm -lmpfr -lgmp \
-lgmpxx
[user@localhost foo]$ ./qc_simple_example
The initial state is
1.0000000e+00|000><000|
Now we apply H to the 0th qubit.
Now we apply CNOT to the qubits 0 and 2.
At this point, the reduced density matrix of \
the qubits 0 and 2 is
5.0000000e-01|00><00|+5.0000000e-01|00><11|\
+5.0000000e-01|11><00|+5.0000000e-01|11><11|
```

Besides this example, the package of ZKCM_QC has sample programs for simulating Grover's quantum search [38] and simulating a simple projective measurement. In addition, we will see an example to simulate the quantum

search under the simplest setting in Appendix A.1, which is written as a part of the explanation of how to handle a three-qubit gate in an MPS simulation.

4.3. Source of numerical errors in an MPS simulation of quantum computing

It is a standard strategy in the MPS simulation and related methods in computational condensed matter physics to impose a certain threshold m_{trunc} to the number of Schmidt coefficients; only larger m_{trunc} Schmidt coefficients (and corresponding Schmidt vectors) are employed and the remaining are discarded at each time when tensors are updated [13, 14]. It has been tacitly assumed that truncations are the main source of numerical errors and a numerical error due to precision shortage has not gathered attention. Venzl *et al.* [33] pointed out that hardness of a time-dependent MPS simulation depends on the distribution of Schmidt coefficients. They reported certain parameter choices in the tilted Bose-Hubbard model, for which the distribution has a rather long tail for larger Schmidt coefficients, *i.e.*, negligibly small ones are not dominant. In such a case, m_{trunc} should be rather close to the maximum Schmidt rank (over all splittings between consecutive sites and over all time steps) in order to keep the truncation error small. In contrast, a usual time-dependent MPS simulation for other nearest-neighbour coupling models studied so far uses a relatively small value for m_{trunc}, typically fifty to one hundred [35]. With this much value of m_{trunc}, a time-dependent MPS simulation usually does not exhibit notable accumulation of numerical errors unless more than several hundred time steps of evolution is tried [35]. A significant accumulation of truncation errors were reported for a larger number of time steps [35, 36].

As mentioned before, it has been uncommon to use truncations in (time-dependent) MPS simulations of quantum computing [12, 19, 27]. This is reasonable because quantum algorithms involves many H and CNOT operations (see Sec. 4.2 for their definitions). This makes a quantum state evolving under a quantum circuit quite often a nearly equally biased superposition of several indices. By tracing-out some subsystem under this condition, we have a reduced density matrix whose nonzero eigenvalues are all nonnegligible. Thus it is not possible to truncate out even a single nonzero Schmidt coefficient, irrespective of the number of time steps. In addition, we have recently shown [37] that an accumulation of errors due to precision shortage is significant even without truncation of nonzero Schmidt coefficients as far as we have seen in an example to iterate the quantum search routine [38]. Thus high-precision computation has a practical advantage in an MPS simulation for a quantum circuit model with a large circuit depth.

Here, we show a typical example where truncating out at most a single nonzero Schmidt coefficient for each time causes a significant error. In this example, slightly more than double precision is required for a stable simulation although the depth of the quantum circuit is not very large.
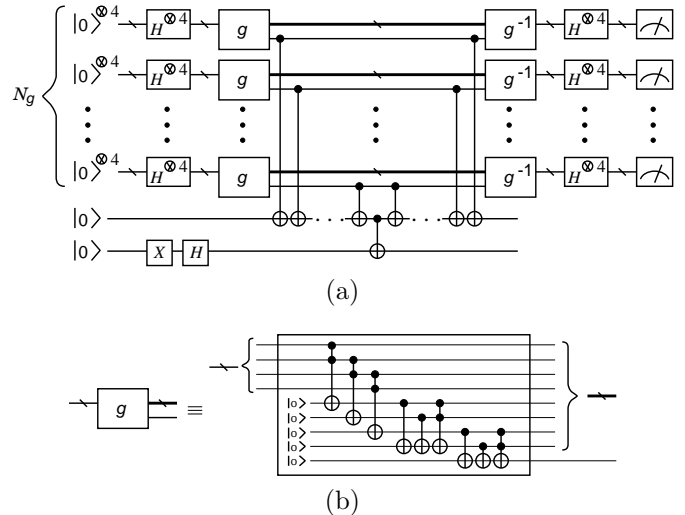

Figure 3: (a) Quantum circuit of the Deutsch-Jozsa algorithm for the specified function (see the text). (b) Internal structure of gate g. Gate g^{-1} is the reverse of g.

We consider the Deutsch-Jozsa algorithm [39]. In a brief explanation, there is a promise that function $f : \{0, 1\}^l \to \{0, 1\}$ is either balanced (*i.e.*, $\#\{\mathbf{x}|f(\mathbf{x}) = 0\} = \#\{\mathbf{x}|f(\mathbf{x}) = 1\}$) or constant (*i.e.*, $f(\mathbf{x})$ is same for all $\mathbf{x}$) where $\mathbf{x} \in \{0_0 \cdots 0_{l-1}, \ldots, 1_0 \cdots 1_{l-1}\}$. The task is to decide whether a given function f is balanced or constant. This takes $1 + 2^{l-1}$ queries for the worst case in classical computation while it takes only a single query in quantum computation with the Deutsch-Jozsa algorithm. The algorithm is described as follows: (i) Apply $H^{\otimes l}V_f H^{\otimes l}$ to l qubits initially in the state $|0_0 \cdots 0_{l-1}\rangle$ where V_f is an operation to put the factor $(-1)^{f(\mathbf{x})}$ to each $|\mathbf{x}\rangle$; (ii) Measure the l qubits in the computational basis. When f is balanced, the probability of finding the qubits simultaneously in 0's in this measurement vanishes; when f is constant, it is exactly unity. For the details of the theoretical analysis of the algorithm, see, *e.g.*, Sec. 3.1.2 of Ref. [10].

Let us consider a particular function $f(\mathbf{y}_0 \cdots \mathbf{y}_{N_g-1}) = \bigoplus_{i=0}^{N_g-1} g(\mathbf{y}_i)$ with $g(x_0x_1x_2x_3) = (x_0 \wedge x_1) \vee (x_1 \wedge x_2) \vee (x_2 \wedge x_3)$ where $\mathbf{y}_i \in \{0, 1\}^4$ and $x_j \in \{0, 1\}$; N_g is a positive integer (here, symbol $\bigoplus$ stands for the exclusive OR operation). Figure 3 shows the quantum circuit of the algorithm for this function. This function is balanced for any value of $N_g \geq 1$. In the figure, a single $\bullet$ and the connected $\oplus$ represent the CNOT operation with the control qubit specified by $\bullet$ and the target qubit specified by $\oplus$. It flips the target qubit if the control qubit is in $|1\rangle$. Similarly, two $\bullet$'s and $\oplus$ connected to each other represent the CCNOT operation. It flips the target qubit if the two control qubits are in $|11\rangle$. (See also Appendix A for the implementation of three-qubit operations in our library.) By the structure of the circuit, each of the N_g measurements should report Prob(0000) = 0 if there is no numerical error. (This is easily proved: assuming different

values of Prob(0000) for two different bundles of qubits contradicts to the fact that the bundles are equivalent to each other by the circuit structure.)

It is straight-forward to write a program code for the quantum circuit using the ZKCM_QC library. We begin with header file descriptions:

```
#include <zkcm_qc.hpp>
#include <sys/time.h>
```

The second header file is needed by the following function to obtain the current time in seconds:

```
double current_time_in_sec ()
{
  timeval T;
  ::gettimeofday(&T, NULL);
  return ((double)(T.tv_sec)
          + 1.0e-6 * (double)(T.tv_usec));
}
```

We use this function when we record the data of time consumption for Table 7. We may omit it otherwise. The main function begins with

```
int main (int argc, char *argv[])
{
  zkcm_set_default_prec (prec);
```

with some precision "`prec`" and ends with

```
  zkcm_quit();
  return 0;
}
```

We describe the quantum circuit step by step in the middle part of the main function. (We call "`current_time_in_sec()`" before and after this part to calculate the time consumption.) First of all, an object of the MPS data structure for $n = 9N_g + 2$ qubits is created by

```
mps M(n);
M.set_m_trunc(mtrunc);
```

where we also set the value of m_{trunc} by our option as in the second line. Then we write each gate operation one by one. For example, a Pauli X gate (or a bit flip) acting on the ith qubit is written as

```
M.applyU(tensor2tools::PauliX, i);
```

Similarly, an Hadamard gate operation is written in the same manner with `tensor2tools::Hadamard`. A CNOT gate with control qubit c and target qubit t is written as

```
M.applyU(tensor2tools::CNOT, c, t);
```

A CCNOT operation with control qubits a, b, and target qubit t is written as

```
M.CCNOT(a, b, t);
```

After writing instructions corresponding to individual quantum gate operations, we need some code lines to obtain the probability of finding zeros in the output. Although we have a function to perform a projective measurement acting on a single qubit, this is not convenient. We instead compute the $(0, 0)$ element of the reduced density matrix of qubits of our interest. To obtain $\text{Prob}(0_0 0_1 0_2 0_3)$, for example, we write

```
std::cout << "Prob(0_0 0_1 0_2 0_3)="
          << M.RDO_block(0, 3).get(0, 0)
          << std::endl;
```

In this way, one can easily write a program code for the quantum circuit.

In the present context, it is also demanded to see the intrinsic data of the MPS step by step. To obtain the number m_s of surviving Schmidt coefficients $V_s(v_s)$ for the splitting between sites s and $s + 1$, one may write, e.g.,

```
int num = M.get_m(s);
```

for some integer $0 \le s \le n - 2$. In addition, each Schmidt coefficient is accessible by "`M.V(s)(i)`" which is a reference to the ith element of V_s. It is also convenient to use "`M.get_m_max()`" ($m_{\max} = \max_s m_s$ for the current time step) and "`M.get_m_maxmax()`" ($m_{\max,\max} = \max_t \max_s m_s$ where t stands for time) so as to find the time step where the Schmidt rank reaches the maximum. It should be noted that sometimes the maximum Schmidt rank appears during the internal process hidden behind each gate operation. This is because each gate operation for nonconsecutive qubits needs to internally move them to consecutive places before operation and move them back to their original places after operation owing to the one-dimensional data structure of MPS. This is done by swapping consecutive qubits step by step. For tracing the internal time evolution of m_s's, one needs to mimic this process by using the operation "`M.SWAP(a,b);`" (this swaps specified qubits a and b) manually.

We have explained how the program code is written to simulate the quantum circuit of Fig. 3. Now we set N_g to 7; we have 65 qubits in total in the circuit. It is certainly intractable to handle the circuit by the brute-force method because the dimension of the Hilbert space is $2^{65} \simeq 3.69 \times 10^{19}$. It was numerically found, however, that the largest possible Schmidt rank of the MPS during evolution in the circuit is only 28 as shown in Fig. 4. Because of this reason, the MPS simulation of the algorithm took only approximately seven minutes (see Table 7) when the precision was set to 256 [bits] and no truncation of nonzero Schmidt coefficients was employed. Here, we used a computing server with the Red Hat Enterprise Linux 6 64-bit OS, Intel Xeon E7-8837 2.67GHz (2.80GHZ maximum) CPU, and 315GB RAM, instead of the common PCs that we normally used.[6]

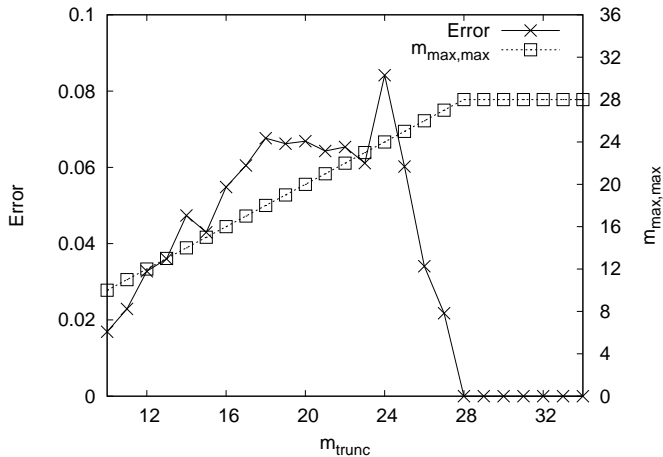[6]This was because a PC with 4GB RAM became unstable due to

Figure 4: Error in the computed value of $\mathrm{Prob}(0_0 0_1 0_2 0_3)$ and $m_{\mathrm{max,max}}$ as functions of m_{trunc}. Precision was fixed to 256 bits.

The main aim of the simulation is to investigate if any truncation of nonzero Schmidt coefficients is possible. Figure 4 shows the error in the computed value of $\mathrm{Prob}(0_0 0_1 0_2 0_3)$ (the discrepancy from zero) as a function of m_{trunc}. The maximum Schmidt rank $m_{\mathrm{max,max}}$ observed during the simulation is also plotted in the figure as a function of m_{trunc}. It is clearly shown that m_{trunc} should be equal to or more than the exactly maximum Schmidt rank that is observed in the absence of truncations; otherwise a significant numerical error appears. (In Ref. [37], we have shown a similar result for a smaller circuit of the algorithm for a different balanced function.) As previously mentioned, the distribution of nonzero Schmidt coefficients is closely related to this phenomenon. We show the distribution in Fig. 5, which was taken at the point where the second CNOT gate was being processed among the $2N_g+1$ CNOT gates in the middle part of Fig. 3(a). It clearly depicts that none of the nonzero Schmidt coefficients was negligible.

In addition, it was found that precision slightly more than the double precision was required to perform a stable simulation even when we did not impose any truncation of nonzero Schmidt coefficients, as shown in Table 7. For precision less than or equal to 55 bits, some of matrix diagonalization routines failed after the half point of the circuit, which indicates an accumulated error due to precision shortage. More specifically speaking about this case, a small non-Hermitian fraction due to the accumulated error in a reduced density matrix resulted in the convergence error of eigenvectors during an update of tensors.

Figure 5: Distribution of nonzero Schmidt coefficients at the point where the second CNOT gate was being processed among the $2N_g+1$ CNOT gates (N_g was set to 7) in the middle part of Fig. 3(a). Note that we are employing the definition of Schmidt coefficients with square roots in this paper. Thus the sum of squared values of the Schmidt coefficients equals to one.

Table 7: Precision (prec) dependence of the numerical error (Error) in the computed value of $\mathrm{Prob}(0_0 0_1 0_2 0_3)$. No truncation of nonzero Schmidt coefficients was employed. The real time consumed for the simulation is also shown (Time), which is an average over 10 trials of the same simulation (the standard deviation is shown in the parentheses). The simulated circuit had 65 qubits because N_g was set to 7. Environment: Red Hat Enterprise Linux 6 64-bit OS, Intel Xeon E7-8837 2.67GHz (2.80GHZ maximum) CPU, and 315GB RAM.

prec	Error	Time [sec]
≤ 55	Convergence failure in some of eigenvectors	N/A
56	1.80×10^{-32}	341 (10.4)
57	5.66×10^{-26}	335 (10.2)
58	1.72×10^{-32}	338 (7.82)
59	1.55×10^{-33}	379 (6.45)
60	1.92×10^{-34}	348 (13.3)
$\vdots$	$\vdots$	$\vdots$
256	5.91×10^{-139}	416 (8.50)
$\vdots$	$\vdots$	$\vdots$
512	7.16×10^{-121}	709 (19.0)
$\vdots$	$\vdots$	$\vdots$
768	1.78×10^{-460}	922 (19.7)
$\vdots$	$\vdots$	$\vdots$
1024	6.50×10^{-615}	1620 (12.3)
$\vdots$	$\vdots$	$\vdots$
1280	7.77×10^{-770}	2170 (16.9)

memory shortage for this simulation for precision ≥ 1024 bits. Each run of the simulation in the computing server consumed at most approximately 8GB memory space for precision 1024 bits and 1280 bits.
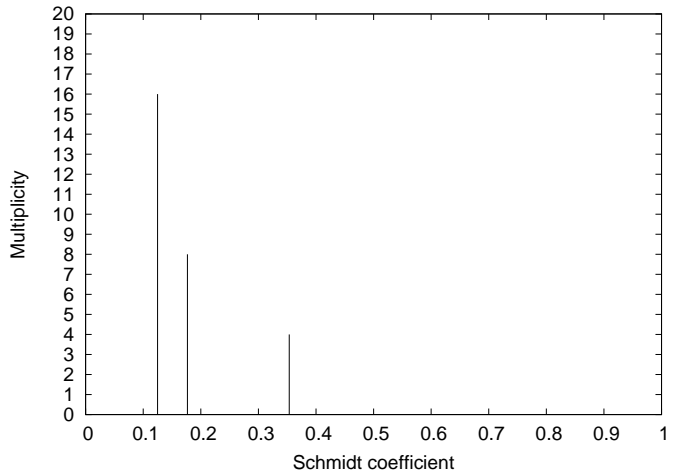
5. Discussion

5.1. Discussion on the ZKCM library

With the ZKCM library, standard tasks in numerical matrix calculations can be completed within the time consumption on the same order of magnitude as that with the PARI library as we have seen in the comparison performed in Sec. 3. The comparison also showed that ZKCM is slower than PARI, even in a simple matrix multiplication, which suggests that basic arithmetic operations make a certain gap in speed of the two libraries. In fact, ZKCM uses MPFR functions while PARI uses GMP functions for the basic arithmetic computation. MPFR is approximately two and a half times as slow as GMP in multiplying floating-point numbers as far as we tested.[7] Thus it is reasonable to find a certain gap in computational speed. We believe the gap is acceptable as long as it does not change the order of magnitude of computation time for basic matrix computation. It has been probably a historical reason that PARI has not used MPFR so far.[8] We chose MPFR because it has floating-point exceptions and other useful functionalities for real floating-point numbers by default.

The only unexpected result in Sec. 3 is the one about Hermitian matrix diagonalization shown in Tables 3 and 4. It has been shown that time consumptions of functions "diag_H" of ZKCM and "eigen" and "jacobi" of PARI are on the same order of magnitude. This is an unusual result because the Jacobi method employed in "jacobi" looks as fast as a variant of the QR method employed in "diag_H" for a 100×100 matrix.

It is likely that "diag_H" and "jacobi" are used for a similar purpose or under a similar situation, since they both work fine for a matrix with degenerate eigenvalues. (It is known [29] that "eigen" almost always fails for a matrix with degenerate eigenvalues.) In this point of view, too, it is meaningful to compare "diag_H" and "jacobi".

As mentioned above, function "jacobi" of PARI is an implementation of a standard Jacobi method. Function "diag_H" of ZKCM employs the Householder-QR method with the Wilkinson shift for computing approximate eigenvalues and uses several sets of inverse iterations to find eigenvectors and at the same time to enhance the accuracy of eigenvalues. It has been commonly known that the Jacobi method is slower than the QR method: "For matrices of order greater than about 10, however, the algorithm is slower, by a significant constant factor, than the QR method..."—page 571 of Ref. [30]; "...the Jacobi method is several times slower than a reduction to tridiagonal form, followed by Francis's algorithm."—page 488 of Ref. [40]. Thus, it is unusual that, for a relatively large matrix with the order 100, there is no significant advantage in using the Householder-QR method. In a phenomenological explanation, this is due to the large cost of inverse iterations. By using the Gprof program [41] (a monitoring software), it turned out that, in "diag_H", more than 71.1 percent of running time was spent for the inverse iterations in case of a 100×100 matrix with the precision ≥ 512 [bits]. In fact speedup of one or two orders of magnitude was possible by omitting inverse iterations for finding eigenvalues as we have shown in Tables 5 and 6. It was however impossible to achieve a required precision without inverse iterations as clearly shown in the tables.

Thus, it was unexpectedly expensive to achieve a sufficient convergence by inverse iterations. We, of course, used the LU decomposition to reduce the cost of each inverse iteration. This, however, did not mitigate the total cost of the inverse iterations sufficiently. As a matter of fact, the total number of the inverse iterations had to be increased along with the increase in required precision. This, at a glance, does not look in accordance with a conventional theory of inverse iteration [42] suggesting that the machine epsilon does not make a difference in the process of inverse iteration. The conventional theory, however, considers the process where the inverse iteration is used for computing an eigenvector for a given approximate eigenvalue. In our case, in contrast, we also improve accuracy of the eigenvalue using the computed eigenvector. A routine of inverse iteration is often called several times in order for achieving sufficient accuracy for each pair of an eigenvalue and the corresponding eigenvector. Furthermore, program routines called by the routine of inverse iteration are not error-free in practice. Thus it was not surprising that the choice of precision considerably affected the cost of inverse iterations (and hence the time consumption of "diag_H" shown in Table 5).

Another factor that makes inverse iterations expensive is the cost of basic arithmetic operations in multiprecision computing. Unlike double-precision computing where every basic arithmetic instruction is performed within a few clock cycles, it takes quite many cycles.[9] It is fast in double-precision computing to successively perform arithmetic instructions because this does not involve any conditional branching. In contrast, it is inevitable to involve several conditional branching instructions in every arithmetic operation in multiprecision computing. Thus, the simple fact that basic arithmetic instructions are not hardware instructions should be a large factor.

---

[7]We wrote a test program to compute $x \longleftarrow x * y$ with $y = 1.00 - 1.00 \times 10^{-7}$ for 10^8 times where the initial value of x was set to 1. The precision was set to 512 bits. It took 15.3 seconds on average (with standard deviation 1.09×10^{-1}) when we used MPFR's "mpfr_t" structure for floating point numbers while it took only 6.11 seconds on average (with standard deviation 4.91×10^{-2}) when we used GMP's "mpf_t" structure. The average was taken over ten trials. This test was performed on a machine with the Fedora 15 64-bit OS, Intel Core i5 M460 CPU, and 4GB RAM. GMP version 4.3.2 and MPFR version 3.0.0 were used.

[8] PARI has been developed since 1979 [24]. GMP appeared in 1991 [8] and MPFR appeared in 2000 [9]. PARI already had plenty of fast floating-point functionalities at the time MPFR appeared.

[9]Theoretically, each instruction with precision prec takes $O(\text{prec}^c)$ time with $c \leq 2$ dependent on the chosen algorithm. In real CPU time, it should scale slightly better in practice because of vectorization of operands. See the manual of GMP [8] for the details of algorithms for arithmetic instructions.

In future, we should find a strategy for faster Hermitian matrix diagonalization. As a possible approach, the precision of computation for finding approximate eigenvalues can be internally enlarged so that a relatively small number of subsequent inverse iterations should be enough to achieve a required precision. Table 5, however, shows that accuracy of approximate eigenvalues is not very much enhanced by simply increasing the preset precision in the Householder-QR method. So far, the author could not find the reason of this tendency. A detailed theoretical and practical analyses of the present implementation (and perhaps the method itself) will be required to overcome this difficulty. For another approach, there is a possibility that a certain method uncommon under the double-precision environment possesses an advantage under a high-precision environment in a practical sense. It is of interest to re-investigate practical usefulness of conventional methods [43] for eigenvalue problems under a high-precision environment.

Apart from computational speed, the syntax of a library is also important for usability. As a C++ library, ZKCM provides an easy-to-use syntax for handling matrices by operator overloading. It also provides various functionalities for matrix computation as member functions of a class as well as as external functions. Thus a program code using the library should look simpler than those written with some other multiprecision libraries for Fortran or C languages. In general, it is relatively easy to write an extension library of a C++ library. As we have introduced, ZKCM has an extension library named ZKCM_QC developed for a (time-dependent) MPS simulation of quantum circuits. The main library and the extension are under steady development. Latest development versions can be downloaded from the repositories linked from the URL [7].

5.2. Discussion on the ZKCM_QC library

As for the ZKCM_QC library, it is worth mentioning that multiprecision computation is useful in MPS simulations of quantum computing as discussed in Sec. 4.3. Indeed, truncation errors are dominant whenever truncations of nonzero Schmidt coefficients are employed. It is however uncommon to employ such truncations in simulating quantum computing since they cause an unacceptably large error as we have discussed. As a consequence, the rounding error become the only possible error. In our example, slightly more than double precision was required for reliable MPS simulation. This is true in a different example to simulate quantum search, which is shown in our related contribution [37]. Thus, time-dependent MPS simulation is fragile not only against accumulating truncation errors [35, 36] but also against accumulating rounding errors. High-precision computation is therefore beneficial to the MPS method.

Apart from the MPS method, there have been several simulators of quantum computing which make use of parallel programming techniques [44, 45, 46, 47] to mitigate the time consumption of the brute-force method. They use a parallelized exact matrix computation and spend a massive computational resource (*e.g.*, more than one thousand CPU processes and several hundred gigabytes physical memory to handle less than forty qubits [45]). It seems that an accumulation of rounding errors is not significant for these simulators although they use double precision computation, as this was not reported so far. In contrast to their approach, use of the MPS method is quite economical. As we have shown in Sec. 4.3, we could handle 65 qubits in the MPS simulation of the Deutsch-Jozsa algorithm under a certain setup, which ran as a single CPU process[10] and took only (approximately) seven minutes in case of 256-bit floating-point precision.

Besides the MPS method, Viamontes *et al.*'s method [16, 56, 57] using a compressed graph representation is also quite economical to simulate quantum computation. According to Refs. [16, 57], its compressed data structure is sensitive to rounding errors so that they used multiprecision computation based on the GMP library. The MPS data structure (1) is of course a compressed data structure for which we needed multiprecision computation for stable quantum circuit simulation. It will be interesting to theoretically investigate if a simulation of quantum computing utilizing a compressed data structure generally has a certain inevitable sensitivity to rounding errors.

Finally, we discuss on the computational cost of the MPS method, which is known to grow polynomially in the maximum Schmidt rank $m_{max,max}$ during the simulation [12] as mentioned in Sec. 4.1. It is expected that MPS simulation becomes very expensive for quantum circuits of algorithms for hard problems like those for quantum prime factorization [48] of a large composite number. It has been discussed [49] that large entanglement (this usually leads to a large Schmidt rank) must be involved in quantum prime factorization. So far, Kawaguchi *et al.* [50] found Schmidt rank 92 in a modular exponentiation circuit (this is used in quantum prime factorization) with 35 qubits in their MPS simulation. Nevertheless, it has been neither proved nor numerically verified that $m_{max,max}$ grows exponentially in the number n of qubits as far as the author knows. Although there have been several studies on entanglement during quantum prime factorization [51, 52, 53, 54], they have not reached an answer to how entanglement grows in n. It is still an open problem how we rigorously estimate the value of $m_{max,max}$ for a given quantum circuit. Presently, a known upper bound for $m_{max,max}$ is a function exponentially growing in the number of basic quantum gates overlapping to each other (*i.e.*, those stretching across the same bundle of wires) [55]; this is however not practically useful for a user of the MPS method to estimate the value of $m_{max,max}$ for his/her simulation. More theoretical and numerical efforts are required to understand the scalability of the method.

---

[10]Every simulation with ZKCM or ZKCM_QC shown in this paper was run as a single CPU process.

6. Summary

We have introduced the ZKCM library which is a C++ library developed for multiprecision complex-number matrix computation. It is especially usable for high-precision numerical simulations in quantum physics; it has an easy-to-use syntax for matrix manipulations and helpful functionalities like the tensor-product and tracing-out operations, the discrete Fourier transform, etc. An extension library ZKCM_QC has also been introduced, which is a library for a multiprecision time-dependent matrix-product-state simulation of quantum computing. It enables a user-friendly coding for simulating quantum circuits.

Appendix A. Updating tensors of an MPS for simulating a three-qubit gate operation

The library ZKCM_QC uses three-qubit gates as elementary gates in addition to single- and two-qubit gates. As it is not usually explained in detail how a three-qubit gate is simulated in a time-dependent MPS simulation, a detailed explanation is given here. As for simulations of single- and two-qubit gates, see Refs. [12, 27] for detailed explanations.

Consider the quantum gate

$$U = \sum_{i_l i_{l+1} i_{l+2}=000}^{111} \sum_{k_l k_{l+1} k_{l+2}=000}^{111} u_{i_l i_{l+1} i_{l+2}, k_l k_{l+1} k_{l+2}}$$
$$\times |i_l i_{l+1} i_{l+2}\rangle\langle k_l k_{l+1} k_{l+2}|$$

acting on the three qubits l, $l+1$, and $l+2$. With a focus on the three qubits, the MPS of n qubits can be written as

$$|\Psi\rangle = \sum_{i_l i_{l+1} i_{l+2}=000}^{111} \sum_{v_{l-1},v_l,v_{l+1},v_{l+2}=0,0,0,0}^{m_{l-1}-1,m_l-1,m_{l+1}-1,m_{l+2}-1} \Big[Q_l(i_l, v_{l-1}, v_l)$$
$$\times V_l(v_l) Q_{l+1}(i_{l+1}, v_l, v_{l+1}) V_{l+1}(v_{l+1}) Q_{l+2}(i_{l+2}, v_{l+1}, v_{l+2})$$
$$\times |v_{l-1}^{0,...,l-1}\rangle |i_l\rangle |i_{l+1}\rangle |i_{l+2}\rangle |v_{l+2}^{l+3,...,n-1}\rangle \Big]$$

with $|v_{l-1}^{0,...,l-1}\rangle = V_{l-1}(v_{l-1})|\Phi_{v_{l-1}}^{0,...,l-1}\rangle$ and $|v_{l+2}^{l+3,...,n-1}\rangle = V_{l+2}(v_{l+2})|\Phi_{v_{l+2}}^{l+3,...,n-1}\rangle$, where $|\Phi_{v_{l-1}}^{0,...,l-1}\rangle$ are the Schmidt vectors of the block of qubits $0,...,l-1$ for the splitting between $l-1$ and l, and $|\Phi_{v_{l+2}}^{l+3,...,n-1}\rangle$ are those of the block of qubits $l+3,...,n-1$ for the splitting between $l+2$ and $l+3$.

What we should do as a simulation of applying the quantum gate U to $|\Psi\rangle$ is to update tensors Q_l, V_l, Q_{l+1}, V_{l+1}, and Q_{l+2} to $\widetilde{Q_l}$, $\widetilde{V_l}$, $\widetilde{Q_{l+1}}$, $\widetilde{V_{l+1}}$, and $\widetilde{Q_{l+2}}$, respectively, so that the MPS with the updated tensors represents the resultant state $|\widetilde{\Psi}\rangle$. This process is explained hereafter step by step. (Here is some note on the description: In case $l-1 = -1$, the tensor V_{l-1} should be regarded as unity and the parameter v_{l-1} should be dropped. Similarly, in

case $l+2 = n-1$, the tensor V_{l+2} should be regarded as unity and the parameter v_{l+2} should be dropped.)

The state after U is applied to the qubits l, $l+1$, and $l+2$ can be written as

$$|\widetilde{\Psi}\rangle = \sum_{v_{l-1}} \sum_{v_{l+2}} \sum_{i_l i_{l+1} i_{l+2}} \Theta(i_l, i_{l+1}, i_{l+2}, v_{l-1}, v_{l+2}) \tag{A.1}$$
$$\times |v_{l-1}^{0,...,l-1}\rangle |i_l\rangle |i_{l+1}\rangle |i_{l+2}\rangle |v_{l+2}^{l+3,...,n-1}\rangle$$

with the tensor

$$\Theta(i_l, i_{l+1}, i_{l+2}, v_{l-1}, v_{l+2}) = \sum_{v_l} \sum_{v_{l+1}} \sum_{k_l k_{l+1} k_{l+2}} \Big[$$
$$u_{i_l i_{l+1} i_{l+2}, k_l k_{l+1} k_{l+2}} Q_l(k_l, v_{l-1}, v_l) V_l(v_l)$$
$$\times Q_{l+1}(k_{l+1}, v_l, v_{l+1}) V_{l+1}(v_{l+1}) Q_{l+2}(k_{l+2}, v_{l+1}, v_{l+2}) \Big].$$

First, we are going to compute the tensors $\widetilde{Q_l}(i_l, v_{l-1}, v_l)$ and $\widetilde{V_l}(v_l)$ of the resultant state. The reduced density matrix of qubits $0, ..., l$ calculated from Eq. (A.1) is

$$\rho^{0,...,l} = \sum_{i_l v_{l-1} i'_l v'_{l-1}} \Big[\sum_{i_{l+1} i_{l+2} v_{l+2}} [V_{l+2}(v_{l+2})]^2$$
$$\times \Theta(i_l, i_{l+1}, i_{l+2}, v_{l-1}, v_{l+2}) \Theta^*(i'_l, i_{l+1}, i_{l+2}, v'_{l-1}, v_{l+2}) \Big]$$
$$\times |v_{l-1}\rangle |i_l\rangle \langle v'_{l-1}|\langle i'_l|$$
$$= \sum_{i_l v_{l-1} i'_l v'_{l-1}} \Big[\sum_{i_{l+1} i_{l+2} v_{l+2}} [V_{l+2}(v_{l+2})]^2$$
$$\times \Theta(i_l, i_{l+1}, i_{l+2}, v_{l-1}, v_{l+2}) \Theta^*(i'_l, i_{l+1}, i_{l+2}, v'_{l-1}, v_{l+2})$$
$$\times V_{l-1}(v_{l-1}) V_{l-1}(v'_{l-1}) \Big] |\Phi_{v_{l-1}}\rangle |i_l\rangle \langle \Phi_{v'_{l-1}}|\langle i'_l|$$
$$= \sum_{i_l v_{l-1} i'_l v'_{l-1}} a_{i_l v_{l-1} i'_l v'_{l-1}} |\Phi_{v_{l-1}}\rangle |i_l\rangle \langle \Phi_{v'_{l-1}}|\langle i'_l|$$

with $a_{i_l v_{l-1} i'_l v'_{l-1}} = \Big[\sum_{i_{l+1} i_{l+2} v_{l+2}} \cdots \Big]$. The matrix $\rho^{0,...,l}$ is a $(2m_{l-1}) \times (2m_{l-1})$ matrix. This is now diagonalized to achieve the eigenvalues $\widetilde{\lambda}_{v_l} = [\widetilde{V}_l(v_l)]^2$ and the corresponding eigenvectors $|\widetilde{\Phi}_{v_l}^{0,...,l}\rangle$ under the basis $\{|\Phi_{v_{l-1}}^{0,...,l-1}\rangle |i_l\rangle\}$. Immediately we find the values of $\widetilde{V}_l(v_l)$. We may truncate out negligibly small eigenvalues[11] to reduce $\widetilde{m_l}$ (the updated value of m_l, namely, the number of data in $\widetilde{V}_l$). In addition, we have vector elements $C_l(i_l, v_{l-1}, v_l)$ of just computed eigenvectors:

$$|\widetilde{\Phi}_{v_l}^{0,...,l}\rangle = C_l(i_l, v_{l-1}, v_l)|\Phi_{v_{l-1}}^{0,...,l-1}\rangle |i_l\rangle,$$

from which we can derive

$$\widetilde{Q_l}(i_l, v_{l-1}, v_l) = C_l(i_l, v_{l-1}, v_l)/V_{l-1}(v_{l-1}).$$

---

[11] We should not employ a threshold for the number of eigenvalues as we have discussed in Sec. 4.3.

Thus we have obtained

$$|\widetilde{\Phi}_{v_l}^{0,\ldots,l}\rangle = \widetilde{Q_l}(i_l, v_{l-1}, v_l)|v_{l-1}\rangle|i_l\rangle.$$

Second, we are going to compute the tensors $\widetilde{V_{l+1}}(v_{l+1})$ and $\widetilde{Q_{l+2}}(i_{l+2}, v_{l+1}, v_{l+2})$ from Eq. (A.1). The reduced density matrix of qubits $l+2, \ldots, n-1$ is

$$\rho^{l+2,\ldots,n-1} = \sum_{i_{l+2}v_{l+2}i'_{l+2}v'_{l+2}} \left[\sum_{i_l i_{l+1} v_{l-1}} [V_{l-1}(v_{l-1})]^2 \right.$$

$$\times \Theta(i_l, i_{l+1}, i_{l+2}, v_{l-1}, v_{l+2})\Theta^*(i_l, i_{l+1}, i'_{l+2}, v_{l-1}, v'_{l+2}) \Big]$$

$$\times |i_{l+2}\rangle|v_{l+2}\rangle\langle i'_{l+2}|\langle v'_{l+2}|$$

$$= \sum_{i_{l+2}v_{l+2}i'_{l+2}v'_{l+2}} \left[\sum_{i_l i_{l+1} v_{l-1}} [V_{l-1}(v_{l-1})]^2 \right.$$

$$\times \Theta(i_l, i_{l+1}, i_{l+2}, v_{l-1}, v_{l+2})\Theta^*(i_l, i_{l+1}, i'_{l+2}, v_{l-1}, v'_{l+2})$$

$$\times V_{l+2}(v_{l+2})V_{l+2}(v'_{l+2}) \Big] |i_{l+2}\rangle|\Phi_{v_{l+2}}\rangle\langle i'_{l+2}|\langle\Phi_{v'_{l+2}}|$$

$$= \sum_{i_{l+2}v_{l+2}i'_{l+2}v'_{l+2}} b_{i_{l+2}v_{l+2}i'_{l+2}v'_{l+2}}|i_{l+2}\rangle|\Phi_{v_{l+2}}\rangle\langle i'_{l+2}|\langle\Phi_{v'_{l+2}}|$$

with $b_{i_{l+2}v_{l+2}i'_{l+2}v'_{l+2}} = \left[\sum_{i_l i_{l+1} v_{l-1}} \cdots\right]$. The matrix $\rho^{l+2,\ldots,n-1}$ is a $(2m_{l+2}) \times (2m_{l+2})$ matrix. This is now diagonalized to achieve the eigenvalues $\widetilde{\lambda}_{v_{l+1}} = [\widetilde{V_{l+1}}(v_{l+1})]^2$ and the corresponding eigenvectors $|\widetilde{\Phi}_{v_{l+1}}^{l+2,\ldots,n-1}\rangle$ under the basis $\{|i_{l+2}\rangle|\Phi_{v_{l+2}}\rangle\}$. The values of $\widetilde{V_{l+1}}(v_{l+1})$ are immediately found. We may truncate out negligibly small eigenvalues to reduce $\widetilde{m_{l+1}}$ (the updated value of m_{l+1}). In addition, we have vector elements $C_{l+2}(i_{l+2}, v_{l+1}, v_{l+2})$ of just computed eigenvectors:

$$|\widetilde{\Phi}_{v_{l+1}}^{l+2,\ldots,n-1}\rangle = C_{l+2}(i_{l+2}, v_{l+1}, v_{l+2})|i_{l+2}\rangle|\Phi_{v_{l+2}}^{l+3,\ldots,n-1}\rangle,$$

from which we can derive

$$\widetilde{Q_{l+2}}(i_{l+2}, v_{l+1}, v_{l+2}) = C_{l+2}(i_{l+2}, v_{l+1}, v_{l+2})/V_{l+2}(v_{l+2}).$$

Thus we have obtained

$$|\widetilde{\Phi}_{v_{l+1}}^{l+2,\ldots,n-1}\rangle = \widetilde{Q_{l+2}}(i_{l+2}, v_{l+1}, v_{l+2})|i_{l+2}\rangle|v_{l+2}\rangle.$$

Third, we are going to compute the tensor $\widetilde{Q_{l+1}}(i_{l+1}, v_l, v_{l+1})$. By the definition of this tensor, we have

$$\widetilde{Q_{l+1}}(i_{l+1}, v_l, v_{l+1}) = \frac{\langle\widetilde{\Phi}_{v_l}^{0,\ldots,l}|\langle i_{l+1}|\langle\widetilde{\Phi}_{v_{l+1}}^{l+2,\ldots,n-1}|\widetilde{\Psi}\rangle}{\widetilde{V_l}(v_l)\widetilde{V_{l+1}}(v_{l+1})}$$

$$= \frac{1}{\widetilde{V_l}(v_l)\widetilde{V_{l+1}}(v_{l+1})} \sum_{i_l i_{l+2} v_{l-1} v_{l+2}} \left\{ \left(\langle\widetilde{\Phi}_{v_l}^{0,\ldots,l}|v_{l-1}\rangle|i_l\rangle\right) \right.$$

$$\times \left(\langle\widetilde{\Phi}_{v_{l+1}}^{l+2,\ldots,n-1}|i_{l+2}\rangle|v_{l+2}\rangle\right) \Theta(i_l, i_{l+1}, i_{l+2}, v_{l-1}, v_{l+2}) \Big\}.$$

We substitute the equations

$$\begin{cases} |\widetilde{\Phi}_{v_l}^{0,\ldots,l}\rangle = \widetilde{Q_l}(i_l, v_{l-1}, v_l)|v_{l-1}\rangle|i_l\rangle \\ |\widetilde{\Phi}_{v_{l+1}}^{l+2,\ldots,n-1}\rangle = \widetilde{Q_{l+2}}(i_{l+2}, v_{l+1}, v_{l+2})|i_{l+2}\rangle|v_{l+2}\rangle \end{cases}$$

into the above equation to obtain

$$\widetilde{Q_{l+1}}(i_{l+1}, v_l, v_{l+1}) = \frac{1}{\widetilde{V_l}(v_l)\widetilde{V_{l+1}}(v_{l+1})} \sum_{i_l i_{l+2} v_{l-1} v_{l+2}} \Bigg\{$$

$$[V_{l-1}(v_{l-1})]^2 \widetilde{Q_l}^*(i_l, v_{l-1}, v_l)\widetilde{Q_{l+2}}^*(i_{l+2}, v_{l+1}, v_{l+2})$$

$$\times [V_{l+2}(v_{l+2})]^2 \Theta(i_l, i_{l+1}, i_{l+2}, v_{l-1}, v_{l+2}) \Bigg\}.$$

In this way, we have obtained the updated tensors

$$\widetilde{Q_l}(i_l, v_{l-1}, v_l), \ \widetilde{V_l}(v_l), \ \widetilde{Q_{l+1}}(i_{l+1}, v_l, v_{l+1}),$$

$$\widetilde{V_{l+1}}(v_{l+1}), \text{ and } \widetilde{Q_{l+2}}(i_{l+2}, v_{l+1}, v_{l+2}).$$

The described process to simulate a three-qubit gate is implemented as the function "`applyU8`" in ZKCM_QC. We will see an example to use the function in the following.

Appendix A.1. Example

Here is an example program to use a three-qubit operation. It simulates the simplest case of Grover's quantum search [38]. One may also see the simulation performed in Sec. 4.3 for another example.

For a brief sketch of the quantum search, suppose that there is an oracle function $f : \{0,1\}^n \to \{0,1\}$ that has r solutions $\mathbf{w}$ (namely, strings $\mathbf{w}$ such that $f(\mathbf{w}) = 1$). Classical search for finding a solution takes $O(2^n/r)$ queries. In contrast, the Grover search finds a solution in $O(\sqrt{2^n/r})$ queries. In particular when $n = 4$ and $r = 1$, a single query is enough for the Grover search. For example, consider the parent data set $\{00, 01, 10, 11\}$ and the solution 01 for a certain oracle with a single oracle bit. A single Grover iteration R maps $|s\rangle = \frac{1}{2}(|00\rangle + |01\rangle + |10\rangle + |11\rangle)|-\rangle_o$ to $|01\rangle|-\rangle_o$, where $R = U_s U_f$ with $U_f = 1 - 2|01\rangle\langle01|$ and $U_s = 1 - 2|s\rangle\langle s|$ acts on the left side qubits; $|-\rangle_o = (|0\rangle_o - |1\rangle_o)/\sqrt{2}$ is a state of the oracle qubit (the rightmost qubit). U_f is a unitary operation corresponding to f and U_s is a so-called inversion-about-average operation. To implement U_f and U_s, we utilize the fact that flipping $|-\rangle_o$ changes the phase factor ±1, following a common implementation [11].

Here, we consider a very simple oracle structure, namely that, it flips $|-\rangle_o$ when the left side qubits are in $|01\rangle$ using a very straight-forward circuit interpretation. Note that there is no realistic benefit to perform a search in such a case because we know the solution beforehand. Usually a search is performed because we cannot guess the solutions by the circuit appearance (consider, *e.g*, an instance of a satisfiability problem [58]). The sample program to simulate the Grover search for the present simple case is shown in Listing 3.

```
#include "zkcm_qc.hpp"
int main()
{
  zkcm_set_default_prec(256);
  mps M(3);
```

```cpp
//Prepare the state for the parent data set and
//the initial state of the oracle qubit.
M.applyU(tensor2tools::Hadamard, 0);
M.applyU(tensor2tools::Hadamard, 1);
M.applyU(tensor2tools::PauliX, 2);
M.applyU(tensor2tools::Hadamard, 2);

//Oracle function with the solution 01.
zkcm_matrix U_f(8, 8);
U_f.set_to_identity();
U_f(2, 2) = U_f(3, 3) = 0;
U_f(2, 3) = U_f(3, 2) = 1;

//Inversion-about-average operation
zkcm_matrix U_s(8, 8);
U_s.set_to_identity();
U_s(0, 0) = U_s(1, 1) = 0;
U_s(0, 1) = U_s(1, 0) = 1;
zkcm_matrix H = zkcm_matrix("[1, 1; 1, -1]")
                / sqrt(zkcm_class(2));
zkcm_matrix I = zkcm_matrix("[1, 0; 0, 1]");
H = tensorprod(tensorprod(H, H), I);
U_s = H * U_s * H;//This is 1-2|s><s|.

std::cout << "Initially, Prob(01)="
          << M.RDO_block(0, 1).get(1, 1)
          << std::endl
          << "Go into Grover's iteration..."
          << std::endl;
for (int i = 0; i < 8; i++)
{
  M.applyU8(U_f, 0, 1, 2);
  M.applyU8(U_s, 0, 1, 2);
  std::cout << "After " << i + 1
            << " times iteration, Prob(01)="
            << M.RDO_block(0, 1).get(1, 1)
            << std::endl;
}
zkcm_quit();
return 0;
}
```

Listing 3: simple_q_search.cpp

The program is compiled and executed in the following way.

```
[user@localhost foo]$ c++ -o simple_q_search \
simple_q_search.cpp -lzkcm_qc -lzkcm -lmpfr \
-lgmp -lgmpxx
[user@localhost foo]$ ./simple_q_search
Initially, Prob(01)=2.500000000e-01
Go into Grover's iteration...
After 1 times iteration, Prob(01)=1.000000000e+00
After 2 times iteration, Prob(01)=2.500000000e-01
After 3 times iteration, Prob(01)=2.500000000e-01
After 4 times iteration, Prob(01)=1.000000000e+00
After 5 times iteration, Prob(01)=2.500000000e-01
After 6 times iteration, Prob(01)=2.500000000e-01
After 7 times iteration, Prob(01)=1.000000000e+00
After 8 times iteration, Prob(01)=2.500000000e-01
```

We see that the success probability, *i.e.*, the probability to find 01 in the left side qubits if we measure them in the computational basis, is unity after a single R is applied. By continuing the iteration, the success probability oscillates.

We have seen a sample program that uses a three-qubit gate by calling the function "applyU8". In addition to this function, there are functions for typical three-qubit gates. They are briefly mentioned below.

Appendix A.2. Typical three-qubit gates

The first typical three-qubit gate is the CCNOT gate already introduced in Sec. 4.3, which flips a single target qubit t under the condition that two control qubits a and b are in $|11\rangle$. ZKCM_QC has a particular member function (of class "mps") for it: "mps & mps::CCNOT (int a, int b, int t);". The second typical one is the controlled-SWAP (CSWAP) gate, which swaps two target qubits p and q under the condition that the control qubit c is in $|1\rangle$. The member function corresponding to this gate is "mps & mps::CSWAP (int c, int p, int q);".

In summary of this appendix, the process to simulate a three-qubit gate operation in a time-dependent MPS simulation has been theoretically described. A sample program to simulate a simple quantum search has been provided, which uses one of the three-qubit gate functions of the ZKCM_QC library.

References

[1] D.H. Bailey, R. Barrio, J.M. Borwein, High-precision computation: Mathematical physics and dynamics, Appl. Math. Comput. 218 (2012) 10106-10121.

[2] D.M. Smith, Multiple Precision Complex Arithmetic and Functions, ACM Trans. Math. Software 24 (1998) 359-367, http://myweb.lmu.edu/dmsmith/FMLIB.html.

[3] B. Haible, R.B. Kreckel, maintainers, CLN - Class Library for Numbers, http://www.ginac.de/CLN/.

[4] D.H. Bailey, Y. Hida, K. Jeyabalan, X.S. Li, B. Thompson, ARPREC, http://crd-legacy.lbl.gov/~dhbailey/mpdist/.

[5] H. Fujiwara, exflib - extend precision floating-point arithmetic library, http://www-an.acs.i.kyoto-u.ac.jp/~fujiwara/exflib/.

[6] M. Nakata, The MPACK (MBLAS/MLAPACK); a multiple precision arithmetic version of BLAS and LAPACK, http://mplapack.sourceforge.net/.

[7] A. SaiToh, ZKCM and ZKCM_QC, http://zkcm.sourceforge.net/.

[8] The GNU Multiple Precision Arithmetic Library, http://gmplib.org/.

[9] L. Fousse, G. Hanrot, V. Lefèvre, P. Pélissier, P. Zimmermann, MPFR: A multiple-precision binary floating-point library with correct rounding, ACM Trans. Math. Software 33 (2007) 13, http://www.mpfr.org/.

[10] J. Gruska, Quantum Computing, McGraw-Hill, 1999.

[11] M.A. Nielsen, I.L. Chuang, Quantum Computation and Quantum Information, Cambridge University Press, 2000.

[12] G. Vidal, Efficient classical simulation of slightly entangled quantum computations, Phys. Rev. Lett. 91 (2003) 147902.

[13] S.R. White, Density Matrix Formulation for Quantum Renormalization Groups, Phys. Rev. Lett. 69 (1992) 2863-2866.

[14] S.R. White, Density-matrix algorithms for quantum renormalization groups, Phys. Rev. B 48 (1993) 10345.

[15] B. Bauer *et al.*, The ALPS project release 2.0: open source software for strongly correlated systems, J. Stat. Mech. 2011(05) (2011) P05001, http://alps.comp-phys.org.

[16] G.F. Viamontes, M. Rajagopalan, I.L. Markov, J.P. Hayes, Gate-Level Simulation of Quantum Circuits, in: Proceedings of the 2003 Asia and South Pacific Design Automation Conference (ASP-DAC 2003), Kitakyushu, Japan, 21-24 Jan. 2003 (ACM Press, New York, 2003) 295-301; G.F. Viamontes, I.L. Markov, J.P. Hayes, Improving Gate-Level Simulation of Quantum Circuits, Quantum Inf. Process. 2 (2003) 347-380.

[17] S. Aaronson, D. Gottesman, Improved simulation of stabilizer circuits, Phys. Rev. A 70 (2004) 052328.

[18] D. Deutsch, A. Barenco, A. Ekert, Universality in quantum computation, Proc. R. Soc. Lond. A 449 (1995) 669-677.

[19] A. Kawaguchi, K. Shimizu, Y. Tokura, N. Imoto, Classical simulation of quantum algorithms using the tensor product representation, e-print arXiv:quant-ph/0411205.

[20] U.W. Kulisch, W.L. Miranker, The arithmetic of the digital computer: A new approach, SIAM Review 28(1) (1986) 1-40.

[21] J.H. Wilkinson, Error analysis of direct methods of matrix inversion, J. ACM 8(3) (1961) 281-330.

[22] L.N. Trefethen, Three mysteries of Gaussian elimination, ACM SIGNUM Newsletter 20(4) (1985) 2-5.

[23] Gnuplot, http://www.gnuplot.info/.

[24] The PARI Group, PARI/GP, (Bordeaux, 2000-2012), http://pari.math.u-bordeaux.fr/.

[25] R. Spira, Calculation of the Gamma function by Stirling's Formula, Math. Comp. 25(114) (1971) 317-322.

[26] M. Kaneko, The Akiyama-Tanigawa algorithm for Bernoulli numbers, J. Integer Seq. 3 (2000) Article 00.2.9.

[27] A. SaiToh, M. Kitagawa, Matrix-product-state simulation of an extended Brüschweiler bulk-ensemble database search, Phys. Rev. A 73 (2006) 062332.

[28] S.A. Smith, T.O. Levante, B.H. Meier, R.R. Ernst, Computer Simulations in Magnetic Resonance. An Object Oriented Programming Approach, J. Magn. Reson. 106a (1994) 75-105, http://gamma.ethz.ch/.

[29] Public communications in the bug tracking system of PARI/GP, Bug report logs - #1349, August 2012.

[30] W.H. Press, S.A. Teukolsky, W.T. Vetterling, B.P. Flannery, Numerical Recipes: The Art of Scientific Computing, 3rd edition, Cambridge University Press, 2007.

[31] D.J. Mueller, Householder's method for complex matrices and eigensystems of Hermitian matrices, Numer. Math. 8 (1966) 72-92.

[32] D. Kressner, Numerical Methods for General and Structured Eigenvalue Problems, Springer-Verlag, 2005.

[33] H. Venzl, A.J. Daley, F. Mintert, A. Buchleitner, Statistics of Schmidt coefficients and the simulability of complex quantum systems, Phys. Rev. E 79 (2009) 056223.

[34] M.C. Bañuls, R. Orús, J.I. Latorre, A. Pérez, P. Ruiz-Femenía, Simulation of many-qubit quantum computation with matrix product states, Phys. Rev. A 73 (2006) 022344.

[35] D. Gobert, C. Kollath, U. Schollwöck, G. Schütz, Real-time dynamics in spin-$\frac{1}{2}$ chains with adaptive time-dependent density matrix renormalization group, Phys. Rev. E 71 (2005) 036102.

[36] J.J. García-Ripoll, Time evolution of Matrix Product States, New J. Phys. 8 (2006) 305.

[37] A. SaiToh, A multiprecision C++ library for matrix-product-state simulation of quantum computing: Evaluation of numerical errors, e-print arXiv:1211.4086.

[38] L.K. Grover, A fast quantum mechanical algorithm for database search, in: Proceedings of the 28th Annual ACM Symposium on Theory of Computing (STOC 1996), Philadelphia, PA, 22-24 May 1996 (ACM Press, New York, 1996) 212-219.

[39] D. Deutsch, R. Jozsa, Rapid solution of problems by quantum computation, Proc. Royal Soc. London A 439 (1992) 553-558.

[40] D.S. Watkins, Fundamentals of Matrix Computations, 3rd edition, Wiley, 2010.

[41] S.L. Graham, P.B. Kessler, M.K. McKusick, gprof: a Call Graph Execution Profiler, in: Proceedings of the 1982 SIGPLAN symposium on Compiler construction, Boston, MA, 23-25 June 1982 (ACM, New York, 1982), ACM SIGPLAN Notices 17(6) (1982) 120-126.

[42] I.C.F. Ipsen, Computing an eigenvector with inverse iteration, SIAM Rev. 39 (1997) 254-291.

[43] Y. Saad, Numerical Methods for Large Eigenvalue Problems, revised edition, SIAM, 2011.

[44] J. Niwa, K. Matsumoto, H. Imai, General-purpose parallel simulator for quantum computing, Phys. Rev. A 66 (2002) 062317.

[45] K. De Raedt, K. Michielsen, H. De Raedt, B. Trieu, G. Arnold, M. Richter, Th. Lippert, H. Watanabe, N. Ito, Massively parallel quantum computer simulator, Comput. Phys. Comm. 176 (2007) 121-136.

[46] F. Tabakin, B. Juliá-Díaz, QCMPI: A parallel environment for quantum computing, Comput. Phys. Comm. 180 (2009) 948-964.

[47] E. Gutiérrez, S. Romero, M.A. Trenas, E.L. Zapata, Quantum computer simulation using the CUDA programming model, Comput. Phys. Comm. 181 (2010) 283-300.

[48] P.W. Shor, Polynomial-time algorithms for prime factorization and discrete logarithms on a quantum computer, SIAM J. Comput. 26 (1997) 1484-1509.

[49] R. Jozsa, N. Linden, On the role of entanglement in quantum-computational speed-up, Proc. R. Soc. Lond. A 459 (2003) 2011-2032.

[50] A. Kawaguchi, K. Shimizu, Y. Tokura, N. Imoto, Classical simulation of the modular exponentiation using the tensor product decomposition, in: Extended Abstract Booklet of the 11th Quantum Information Technology Symposium, Kyoto, Japan, 6-7 December 2004 (unpublished, in Japanese with English abstract) pp.163-166, technical report No. QIT2004-82.

[51] S. Parker, M.B. Plenio, Entanglement simulations of Shor's algorithm, J. Mod. Opt. 49 (2002) 1325-1353.

[52] Y. Shimoni, D. Shapira, O. Biham, Entangled quantum states generated by Shor's factoring algorithm, Phys. Rev. A 72 (2005) 062308.

[53] V.M. Kendon, W.J. Munro, Entanglement and its role in Shor's algorithm, Quantum Inf. Comput. 6 (2006) 630-640.

[54] Y. Most, Y. Shimoni, O. Biham, Entanglement of periodic states, the quantum Fourier transform, and Shor's factoring algorithm, Phys. Rev. A 81 (2010) 052306.

[55] R. Jozsa, On the simulation of quantum circuits, e-print arXiv:quant-ph/0603163.

[56] G.F. Viamontes, I.L. Markov, J.P. Hayes, Graph-based simulation of quantum computation in the density matrix representation, Quantum Inf. Comput. 5 (2005) 113-130.

[57] G.F. Viamontes, Efficient Quantum Circuit Simulation, PhD Thesis, University of Michigan, 2007.

[58] M.R. Garey, D.S. Johnson, Computers and Intractability: A Guide to the Theory of NP-Completeness, W.H. Freeman and Co., 1979.